

TNO Defence Research  
**AD-A273 755**  
■■■■■■■■■■

TNO-report  
FEL-93-A135

copy no.

8

title

Theory and Modeling of Stimulated Raman Scattering

TNO Physics and Electronics  
Laboratory

Oude Waalsdorperweg 63  
2597 AK The Hague  
P.O. Box 96864  
2509 JG The Hague  
The Netherlands

Fax +31 70 328 09 61  
Phone +31 70 326 42 21

①

to 93-1437

author(s):

J.C. van den Heuvel

date:

June 1993

DTIC  
ELECTE  
DEC 15 1993  
S E D

classification

classified by

: A.A.M. Aarssen

classification date

: June 16, 1993

**TDCK**

Frederikkazerne, gebouw 140  
v/d Burchlaan 31 MPC 16A  
TEL. : 070-3166394/6395  
FAX. : (31) 070-3166202  
Postbus 90701  
2509 LS Den Haag **TDCK**

title

: ongerubriceerd

abstract

: ongerubriceerd

report text

: ongerubriceerd

appendices A t/m C

: ongerubriceerd

All rights reserved.

No part of this publication may be reproduced and/or published by print, photoprint, microfilm or any other means without the previous written consent of TNO.

In case this report was drafted on instructions, the rights and obligations of contracting parties are subject to either the 'Standard Conditions for Research Instructions given to TNO', or the relevant agreement concluded between the contracting parties.

Submitting the report for inspection to parties who have a direct interest is permitted.

© TNO

no. of copies : 30

no. of pages : 85 (including appendices, excluding RDP and distribution list)

no. of appendices : 3

All information which is classified according to Dutch regulations shall be treated by the recipient in the same way as classified information of corresponding value in his own country. No part of this information will be disclosed to any party.

The classification designation ONGERUBRICEERD is equivalent to UNCLASSIFIED.

Approved for public release  
Distribution

Netherlands organization for  
applied scientific research

TNO Defence Research consists of:  
the TNO Physics and Electronics Laboratory,  
the TNO Prins Maurits Laboratory and the  
TNO Institute for Perception.



The Standard Conditions for Research Instructions given to TNO, as filed at the Registry of the District Court and the Chamber of Commerce in The Hague shall apply to all instructions given to TNO.

93-30376



93 12 14 08 6

**Best  
Available  
Copy**

## EXECUTIVE SUMMARY

The objective of the research described in this report is the optimization of wavelength conversion of laser radiation. Wavelength conversion of a specific laser is a method to enhance its applicability, since the wavelength of a laser determines its utilization. In particular, the wavelength conversion of the Nd:YAG laser from 1.06  $\mu\text{m}$  to 1.54  $\mu\text{m}$  is attractive since the 1.54  $\mu\text{m}$  is eye-safe in contrast with the eye-hazardous 1.06  $\mu\text{m}$ . For the armed forces, applications are found in laser range finders, trackers, and target indicators, which can be operated safely using 1.54  $\mu\text{m}$  radiation. Since atmospheric transmission at this wavelength is slightly better than for 1.06  $\mu\text{m}$  and detection systems have a higher sensitivity at this wavelength, laser range finders have an enhanced performance at 1.54  $\mu\text{m}$ . Contact with Dutch and International companies has been established for the production of a 1.54  $\mu\text{m}$  laser range finder based on the SRS technology.

We studied the technology of wavelength conversion by the stimulated Raman scattering (SRS) process. Using high pressure methane as a SRS medium, an energy efficiency of 45% was obtained. Due to the difference in photon energy, the theoretical maximum of the energy efficiency is 69%. A numerical model has been developed to assist in the optimization and to analyze the experimental results. Experimental validation of the numerical results has been carried out with success. With the use of the numerical model, it is expected that other wavelength conversions can be optimized faster and less expensive than by the experimental trial-and-error approach.

Conversion to the mid-infrared wavelength of 3.6  $\mu\text{m}$  is under way using a modified Nd:YAG laser at 1.44  $\mu\text{m}$  and converting this wavelength by SRS in hydrogen gas. Application of a 3.6  $\mu\text{m}$  laser is found in ranging and in jamming of sensor systems that operate in the 3-5  $\mu\text{m}$  atmospheric window. With the developed numerical model, the wavelength conversion to 3.6  $\mu\text{m}$  will be optimized.

DTIC QUALITY INSPECTED 1

Accession For	
NTIS	CRA&I
DTIC	TAB
Unannounced	<input type="checkbox"/>
Justification	.....
By .....	
Distribution / .....	
Availability Codes	
Dist	Avail and / or Special
A-1	

report no. : FEL-93-A135  
title : Theory and Modeling of Stimulated Raman Scattering  
  
author(s) : J.C. van den Heuvel  
Institute : TNO Physics and Electronics Laboratory  
  
date : June 1993  
NDRO no. : A90KL674  
no. in pow '93 : -  
  
Research supervised by : R.J.L. Lerou  
Research carried out by : F.J.M. van Putten and J.C. van den Heuvel

---

#### ABSTRACT (ONGERUBRICEERD)

A three-dimensional finite difference method is presented for the propagation through a gain medium of beams focused by an astigmatic lens. The method is used for the modeling of a Raman amplifier that uses astigmatic lenses. With this method, the effect of gain focusing on the amplification is studied. The numerical results show a good correspondence with analytical models in the range where these models are applicable.

The threshold power of stimulated Raman scattering (SRS) has been calculated for various nondiffraction-limited pump beams using the numerical model. It is shown that the threshold power, for a tightly focused beam, depends on the  $M^2$  factor that is related to the pump beam quality. Additionally, the influence of the exact pump beam profile on the threshold is small. Therefore, the  $M^2$  factor is a useful parameter for analyzing the experimental threshold. We show that the measured SRS thresholds in methane correspond with the calculated thresholds.

An astigmatic focus has been used to increase the conversion efficiency of a Raman cell at high pump energy. Experimental and numerical results show that the increased conversion is due to the reduction of cascade second order Stokes. It is shown that other effects, namely Brillouin scattering, anti-Stokes generation, and ground-state depletion are negligible for our experimental setup.

rapport no. : FEL-93-A135  
titel : Theorie en Modellerings van Gestimuleerde Raman Verstrooiing  
  
auteur(s) : Dr. J.C. van den Heuvel  
instituut : Fysisch en Elektronisch Laboratorium TNO  
  
datum : juni 1993  
hdo-opdr.no. : A90KL674  
no. in lwp '93 : -  
  
Onderzoek uitgevoerd o.l.v. : Drs. R.J.L. Lerou  
Onderzoek uitgevoerd door : Ing. F.J.M. van Putten en Dr. J.C. van den Heuvel

---

#### SAMENVATTING (ONGERUBRICEERD)

Een drie-dimensionale numerieke methode op basis van *finite differences* voor de propagatie door een versterkend medium van bundels gefocuseerd met een astigmatische lens wordt besproken. De methode wordt gebruikt voor de modellering van een Raman cel met astigmatische lenzen. Het effect van *gain focusing* op de versterking wordt met het model onderzocht. De numerieke resultaten komen overeen met analytische modellen voor het gebied waar deze geldig zijn.

Het *threshold* vermogen van gestimuleerde Raman verstrooiing (SRS) is berekend voor diverse niet-diffractie-begrensde pompbundels m.b.v. het numerieke model. Er wordt aangetoond dat het threshold vermogen voor een gefocuseerde pompbundel afhangt van de  $M^2$  factor die een maat is voor de bundelkwaliteit. Daarbij blijkt de invloed van het precieze pompbundel profiel op het threshold vermogen gering te zijn. Hierdoor is de  $M^2$  factor een bruikbare parameter voor de analyse van de experimentele threshold. We tonen aan dat de gemeten SRS thresholds in methaan overeenkomen met de berekende thresholds.

Een astigmatisch focus is gebruikt om het conversie rendement van een Raman cel te verhogen bij hoge pompenergieën. Experimentele en numerieke resultaten laten zien dat het toegenomen rendement te danken is aan de afname van cascade tweede orde Stokes. Er wordt aangetoond dat andere effecten als Brillouin verstrooiing, anti-Stokes productie, en depletie van de grondtoestand te verwaarlozen zijn voor onze experimentele opstelling.

<b>EXECUTIVE SUMMARY</b>	<b>2</b>
<b>ABSTRACT</b>	<b>3</b>
<b>SAMENVATTING</b>	<b>4</b>
<b>CONTENTS</b>	<b>5</b>
<b>1 INTRODUCTION</b>	<b>7</b>
<b>2 THEORY OF NUMERICAL SIMULATION</b>	<b>10</b>
2.1 Introduction	10
2.2 Beam propagation method	11
2.3 Plane-wave model	21
2.4 Results and Discussion	26
2.5 Summary and Conclusions	33
<b>3 EXPERIMENTS USING METHANE</b>	<b>34</b>
3.1 Experimental setup	34
3.2 Methane parameters	36
3.3 Beam quality measurements	37
<b>4 THRESHOLD OF STIMULATED RAMAN SCATTERING</b>	<b>41</b>
4.1 Introduction	41
4.2 Theory	42

4.3	Results and Discussion	45
4.4	Conclusions	53
5	OPTIMIZATION OF CONVERSION EFFICIENCY	55
5.1	Introduction	55
5.2	Theory	56
5.3	Experiment	58
5.4	Results and Discussion	60
5.5	Conclusions	65
6	CONCLUSIONS	67
	REFERENCES	69
	APPENDIX A RUNNING THE PROGRAM	
	APPENDIX B LIST OF INPUT PARAMETERS	
	APPENDIX C DETAILS OF THE PROGRAM	

## 1 INTRODUCTION

Wavelength conversion by stimulated Raman scattering (SRS) has been used to generate new wavelengths from existing efficient lasers [1]. In particular, the conversion of Nd:YAG radiation at  $1.064\text{ }\mu\text{m}$  to  $1.543\text{ }\mu\text{m}$  by SRS in methane has been studied at our laboratory. The  $1.543\text{ }\mu\text{m}$  radiation has the advantage over  $1.064\text{ }\mu\text{m}$  that it is eye-safe since the radiation is strongly absorbed by the eye's interior before reaching the retina [2]. Subsequently, we shall use the terms pump beam and Stokes beam for the original laser beam and the wavelength shifted beam. In this report, the theory of SRS and the modeling of the wavelength conversion is described. More information on the experimental setup and experimental results can be found in the reports: FEL-90-B098 (in Dutch) and FEL-92-A125 [3,4].

Chapter 2 describes the numerical model that has been developed at our laboratory to study and to optimize wavelength conversion of laser radiation by SRS. The extension to an astigmatic focus is included in the numerical model for the analysis of our experiments with astigmatic lenses. These experiments showed that the use of an astigmatic lens or a pair of cylindrical lenses can increase the conversion efficiency of a Raman amplifier [3]. Because of the astigmatic focus, the gain medium is no longer rotationally symmetric, so a single radial coordinate cannot be used. Therefore, a two dimensional grid is used for the finite difference (FD) method, and this grid is propagated along the optical axis resulting in three space dimensions. Previous studies have shown that there is a narrowing of the Stokes beam because of the higher amplification at the center of the pump beam [5,6,7]. This effect is called gain focusing and the analytical model describing it [6] is compared with our numerical results.

Threshold measurements and simulations are described in chapter 4. The SRS process has no real threshold like a laser, but an experimental threshold can be defined. Here the threshold stands for the pump power corresponding to 1 percent conversion efficiency. In this chapter we study the effect of pump beam quality on the threshold power. By changing the diaphragm inside the laser, we could change the quality of the output beam. Because the pump beam is focused into the Raman medium, the SRS process will depend on its beam quality since the process is driven by the intensity at the focus, which is high for a good beam quality and decreases with decreasing beam quality.

The beam quality is related to the  $M^2$  factor, which is a dimensionless factor that compares

the divergence of a given beam with the divergence of a (diffraction-limited) Gaussian beam. The divergence of an arbitrary beam can be defined unambiguously using the variances  $\sigma_x^2$  and  $\sigma_y^2$  of the beam profile in the two transverse directions. By comparing the rate of increase of the variance of an arbitrary beam (i.e. the divergence) with the corresponding rate of a Gaussian beam with the same waist width, the  $M^2$  factor can be determined. This  $M^2$  factor is a fundamental property of the beam which is not changed by a lens if the lens has a sufficient diameter to avoid truncation of the beam profile and negligible spherical aberration [8]. In fact, the  $M^2$  determines the intensity at the lens focus and the length of the focus; the product of these quantities is a factor  $1/M^2$  lower compared to a TEM<sub>00</sub> beam.

The amplification of the Stokes beam by a nondiffraction-limited pump beam is solved numerically using our numerical model described in chapter 2. For the nondiffraction-limited pump beam, Gaussian-Hermite (G-H) beams, Gaussian-Laguerre (G-L) beams, and Gaussian-Schell-model (GSM) beams are used. The  $M^2$  factor of these beams can be calculated analytically. A random superposition of G-H modes is also used as a pump beam; for this type of beam, the  $M^2$  factor is obtained numerically.

It is shown that for high amplification (i.e. at threshold power) the gain of the Stokes beam is approximately the same for beam profiles of different type but with the same  $M^2$ . Therefore, the threshold power, i.e. the power at which the Stokes power is 1% of the pump power, depends strongly on the  $M^2$  factor and to a lesser extent on the exact beam profile of the pump. The relation between  $M^2$  and the threshold power was confirmed experimentally in a Raman cell containing high pressure methane.

Chapter 5 describes the optimization of the wavelength conversion at high pump energies by the use of astigmatic lenses or a pair of cylindrical lenses. Approximately, the conversion does not change by varying the focal length of an ordinary lens since the length of the focus times the intensity at the focus is constant [9]. Thus, a shorter focal length results in a shorter Rayleigh range (length of focus) which is compensated by the increased intensity at the focus. However, an astigmatic focus can be used to modify the gain and therefore the conversion. An astigmatic focus gives a tuning facility by varying  $\Delta F$ , i.e. the distance between the two foci.

In the experimental study, a Nd:YAG laser was focused into a Raman cell containing 88 bar of methane. The conversion of the pump beam to other wavelengths was studied as a function of pump energy for an ordinary and for an astigmatic focus. We monitored the energy at the following generated wavelengths: the first Stokes at 1.5  $\mu\text{m}$ , the second Stokes

at 2.8  $\mu\text{m}$ , the anti-Stokes at 0.8  $\mu\text{m}$ , and the Brillouin scattering at 1.06  $\mu\text{m}$ . A dichroic mirror, transparent for the pump and highly reflective for the first Stokes, was placed at the entrance of the cell to enhance the first-Stokes generation.

Numerical simulations were performed and compared with the experimental results. All input parameters were obtained from the literature and none of the parameters were fitted to match the simulations to the experiments. A reasonable agreement between the experiment and the simulation was found. It is shown that the increased conversion efficiency for an astigmatic focus is due to the reduction of second Stokes radiation at 2.8  $\mu\text{m}$ .

## 2 THEORY OF NUMERICAL SIMULATION

### 2.1 Introduction

A numerical model has been developed at our laboratory to study and to optimize wavelength conversion of laser radiation by stimulated Raman scattering (SRS). The extension to an astigmatic focus is included in the numerical model for the analysis of our experiments with astigmatic lenses. These experiments showed that the use of an astigmatic lens or a pair of cylindrical lenses can increase the conversion efficiency of a Raman amplifier [13]. In chapter 5 this improvement of the conversion efficiency for astigmatic lenses is studied further. In this chapter, we present the numerical method in detail and we show some numerical results.

The Stokes beam is amplified in a spatially nonuniform gain medium generated by the focused pump beam. The problem of beam propagation in a rotationally symmetric gain medium has been treated by expanding the pump and the Stokes beam in Gaussian-Laguerre modes and calculating the mode coupling [5,6,7]. These studies have shown that there is a narrowing of the Stokes beam because of the higher amplification at the center of the pump beam. This effect is called gain focusing and the analytical model describing it [6] will be compared with our numerical results.

Because of the astigmatic focus, the gain medium is no longer rotationally symmetric. In this chapter the beam propagation in a non-rotationally symmetric gain medium is studied. A method based on finite differences is used and this method will be described in section 2.2. Since there is no rotational symmetry, both the  $x$  and  $y$  coordinate have to be used instead of a single radial coordinate. Therefore, a two-dimensional grid is used in the finite difference (FD) method. Because the grid is propagated in the  $z$ -direction, the FD method is in effect a three-dimensional model.

The results of the FD method are cross-checked using analytical models. It is shown that for low pump powers the results of the FD method agree with the analytical model of Kung [14,15]. For high powers the effect of gain focusing increases the amplification of the Stokes beam. In the regime of high pump powers, the results of the FD method agree with the analytical model of Cotter et al. [6] that includes gain focusing.

For the analysis of the time dependence of the pump and the Stokes pulse, we have developed a plane-wave model that uses one space and one time coordinate without the two transverse

space coordinates. This method uses the amplification obtained from the FD method, so in this way gain focusing and astigmatism are included. The details of this method will also be presented in section 2.2.

Since the experiments deal with the Stokes energy versus the pump energy, the experimental results are compared with the results of the plane wave model, which include the calculated energies of the pump and the Stokes pulse.

## 2.2 Beam propagation method

### 2.2.1 The paraxial wave equation

The propagation of beams in free space is given by the wave equation

$$\nabla^2 E - \frac{1}{c^2} \partial_t^2 E = 0, \quad (2.1)$$

where  $E$  is the scalar electric field and  $c$  is the speed of light. If we substitute in equation (2.1) the solution for  $E(x, y, z, t)$  of the form

$$E(x, y, z, t) = \mathcal{E}(x, y, z) \exp[ikz - i\omega t] \quad (2.2)$$

and use the slowly varying envelope approximation

$$|\partial_x^2 \mathcal{E}| \ll |2k \partial_x \mathcal{E}|, \quad (2.3)$$

then the paraxial wave equation is obtained

$$\partial_x^2 \mathcal{E} + \partial_y^2 \mathcal{E} + 2ik \partial_z \mathcal{E} = 0. \quad (2.4)$$

The relation  $\omega = ck$  between the angular frequency  $\omega$  and the wave number  $k$  was used in this derivation.

The paraxial wave equation (2.4) is used for the propagation of the Stokes and the pump beam. The Stokes field  $\mathcal{E}_s$  is amplified in a gain medium that is generated by the pump field  $\mathcal{E}_p$ . The paraxial wave equation for the Stokes field is given by [6,16]

$$\partial_x^2 \mathcal{E}_s + \partial_y^2 \mathcal{E}_s + 2ik_s \partial_z \mathcal{E}_s = ik_s g \mathcal{E}_s |\mathcal{E}_p|^2, \quad (2.5)$$

where  $g$  is the Raman gain coefficient. The paraxial wave equation for the pump field, including pump depletion, is given by

$$\partial_x^2 \mathcal{E}_p + \partial_y^2 \mathcal{E}_p + 2ik_p \partial_z \mathcal{E}_p = -i \frac{k_p^2}{k_s} g \mathcal{E}_p |\mathcal{E}_s|^2. \quad (2.6)$$

These two partial differential equations can be considered as an initial value problem (with  $z$  instead of  $t$ ). The Stokes and the pump field at the entrance window of the Raman amplifier are known and solving (2.5) and (2.6) gives us the two fields at the exit window. A FD method is used to solve (2.5) and (2.6) by numerically integrating these equations along the  $z$ -axis. The numerical integration uses the values on a two dimensional grid to represent the cross-section of the Stokes and the pump field.

We shall introduce new transverse coordinates because the FD method needs a grid that is adjusted to the width of the pump beam. Otherwise, only a few grid points are used effectively at the focus. The new transverse coordinates scale to the width of the pump beam and are used to define the grid. The pump beam is focused into the Raman amplifier by an astigmatic lens. If there is no pump depletion and the pump beam is Gaussian, the cross-section of the beam is an ellipse and the widths of the elliptic Gaussian pump beam are given by [17]

$$w_x^2(z) = w_{ox}^2 (1 + (z - z_{fx})^2 / z_{ox}^2) \quad \text{and} \quad (2.7)$$

$$w_y^2(z) = w_{oy}^2 (1 + (z - z_{fy})^2 / z_{oy}^2), \quad (2.8)$$

where in the  $x$ - $z$  plane  $z_{fx}$  is the place of the focus,  $z_{ox}$  is the Rayleigh range ( $2z_{ox}$  is often called the confocal parameter), and  $w_{ox}$  is the half width of the beam at the focus. The parameters for the  $y$ - $z$  plane are analogous to the parameters for the  $x$ - $z$  plane. The equations for the beam width are used to define two new transverse coordinates  $\bar{x}$  and  $\bar{y}$

$$x = w_x(z) \bar{x} \quad \text{and} \quad y = w_y(z) \bar{y}. \quad (2.9)$$

The paraxial wave equations (2.5) and (2.6) can be written in terms of the new transverse coordinates. The equation for the Stokes field with the new transverse coordinates is

$$\begin{aligned} \frac{\partial^2}{w_x^2} \mathcal{E}_s + \frac{\partial^2}{w_y^2} \mathcal{E}_s + 2ik_s (\partial_z \mathcal{E}_s - \bar{x} \partial_x (\ln w_x) \partial_{\bar{x}} \mathcal{E}_s - \bar{y} \partial_y (\ln w_y) \partial_{\bar{y}} \mathcal{E}_s) = ik_s g \mathcal{E}_s |\mathcal{E}_p|^2. \end{aligned} \quad (2.10)$$

As a consequence of the introduction of the new transverse coordinates there appear first order transverse differentials of  $\mathcal{E}_s$ . These differentials might be incorporated in a FD method. However, we will use a transformation that removes the first order transverse differentials. The advantage of this transformation is that the remaining term can be integrated analytically. The first order transverse differentials of  $\mathcal{E}_s$  can be removed by the following transformation:

$$S(\bar{x}, \bar{y}, z) = \mathcal{E}_s(\bar{x}, \bar{y}, z) \times \exp \left[ i \frac{k_s w_{oz}^2}{2 z_{oz}^2} (z_{fz} - z) \bar{x}^2 \right] \exp \left[ i \frac{k_s w_{oy}^2}{2 z_{oy}^2} (z_{fy} - z) \bar{y}^2 \right]. \quad (2.11)$$

The equation for the transformed Stokes field  $S$  is

$$\begin{aligned} \frac{\partial^2}{\partial \bar{x}^2} S + \frac{\partial^2}{\partial \bar{y}^2} S + i k_s \left( \partial_z \ln w_x + \partial_z \ln w_y + i k_s \frac{w_{oz}^2 \bar{x}^2}{z_{oz}^2 + (z - z_{fz})^2} \right. \\ \left. + i k_s \frac{w_{oy}^2 \bar{y}^2}{z_{oy}^2 + (z - z_{fy})^2} \right) S + 2 i k_s \partial_z S = i k_s g S |P|^2. \end{aligned} \quad (2.12)$$

The transformation of the pump field is obtained by replacing  $k_s$  with  $k_p$  in the phase factors. The equation for the transformed pump field  $P$  is

$$\begin{aligned} \frac{\partial^2}{\partial \bar{x}^2} P + \frac{\partial^2}{\partial \bar{y}^2} P + i k_p \left( \partial_z \ln w_x + \partial_z \ln w_y + i k_p \frac{w_{oz}^2 \bar{x}^2}{z_{oz}^2 + (z - z_{fz})^2} \right. \\ \left. + i k_p \frac{w_{oy}^2 \bar{y}^2}{z_{oy}^2 + (z - z_{fy})^2} \right) P + 2 i k_p \partial_z P = -i \frac{k_p^2}{k_s} g P |S|^2. \end{aligned} \quad (2.13)$$

The equations (2.12) and (2.13) will be solved numerically by the FD method that is described below.

## 2.2.2 Description of the finite difference method

The equations for the Stokes and the pump field are solved by a FD method. Since the problem is an initial value problem, the strategy is to integrate stepwise along the  $z$ -axis. The FD method will solve (2.12) and (2.13) using the values on a two dimensional grid to represent the fields at a cross section of the beam. These grid values will be used to compute the fields on these grid points after some step  $\Delta z$  along the  $z$ -axis. This procedure starts at the entrance window and ends at the exit window of the Raman amplifier.

The Stokes and the pump field at the entrance window ( $z = 0$ ) are represented by the values on a two dimensional grid. These grid values are given by

$$s_{l,m}^{n=0} = S(\bar{x}, \bar{y}, z = 0) \quad \text{and} \quad p_{l,m}^{n=0} = P(\bar{x}, \bar{y}, z = 0), \quad (2.14)$$

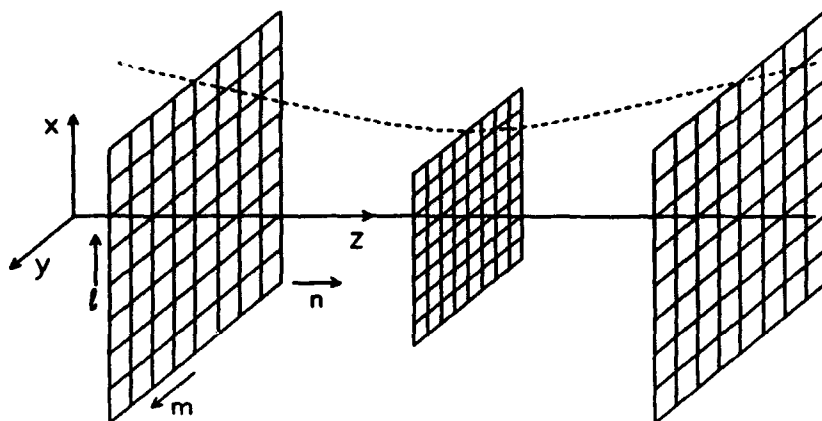


Figure 2.1: Rectangular grid used by the finite difference method. As the grid advances along the  $z$ -axis its width is adjusted to the width of the pump beam.

$$\text{with } \bar{x} = l\Delta\bar{x}, \quad \bar{y} = m\Delta\bar{y}, \quad \text{and} \quad z = n\Delta z. \quad (2.15)$$

The subscripts  $l$  and  $m$  are indices that indicate the position on the grid; the superscript  $n$  is an index that gives the number of integration steps. This grid is advanced along the  $z$ -axis as is illustrated in figure 2.1. The width of the grid is adjusted to the width of the pump beam by using the transverse coordinates  $\bar{x}$  and  $\bar{y}$  instead of  $x$  and  $y$ .

The FD method for the integration along the  $z$ -axis is composed of several distinct methods obtained by splitting the differential equation. This procedure is based on the FD operator splitting method that is used for initial value equations [18]. The equation for the Stokes field is of the form  $\partial_z S = \mathcal{L}S$ , where  $\mathcal{L}$  is some differential operator. This operator can be split into a linear sum of four differential operators

$$\begin{aligned} \partial_z S &= \frac{i}{2k_s w_z^2} \partial_{\bar{x}}^2 S + \frac{i}{2k_s w_y^2} \partial_{\bar{y}}^2 S + \frac{g}{2} S |P|^2 - \frac{1}{2} \left( \partial_z \ln w_z + \partial_z \ln w_y \right. \\ &\quad \left. + ik_s \frac{w_{oz}^2 \bar{x}^2}{z_{oz}^2 + (z - z_{fz})^2} + ik_s \frac{w_{oy}^2 \bar{y}^2}{z_{oy}^2 + (z - z_{fy})^2} \right) S \\ &= \mathcal{L}_1 S + \mathcal{L}_2 S + \mathcal{L}_3 S + \mathcal{L}_4 S. \end{aligned} \quad (2.16)$$

The FD method for the equation  $\partial_z S = \mathcal{L}_i S$  is called  $U_i$ . With these methods  $U_i$ , the method for the total operator is obtained by successively applying these methods  $U_i$  to the

grid values. This means that the method for the total operator is given by

$$\begin{aligned} r^1 &= U_1(s^n) \\ r^2 &= U_2(r^1) \\ r^3 &= U_3(r^2) \\ s^{n+1} &= U_4(r^3) \end{aligned} \quad (2.17)$$

where the  $r^i$  are intermediate grid values that are discarded after completion of the step in  $z$ . The four methods  $U_i$  of (2.17) will be described below.

### 2.2.3 The method for the diffraction

The diffraction of the Stokes beam is given by the second order partial differential equation

$$\partial_z S = \frac{i}{2k_s w_z^2} \partial_z^2 S + \frac{i}{2k_s w_y^2} \partial_y^2 S = \mathcal{L}_1 S + \mathcal{L}_2 S. \quad (2.18)$$

This equation can be split into two operators. The differentials in the equation  $\partial_z S = \mathcal{L}_1 S$  are approximated by finite differences in the following way

$$\frac{s_{l,m}^{n+1} - s_{l,m}^n}{\Delta z} = i \left( \frac{s_{l+1,m}^n - 2s_{l,m}^n + s_{l-1,m}^n}{4k_s w_z^2 (\Delta \bar{x})^2} + \frac{s_{l+1,m}^{n+1} - 2s_{l,m}^{n+1} + s_{l-1,m}^{n+1}}{4k_s w_z^2 (\Delta \bar{x})^2} \right). \quad (2.19)$$

This particular method of using the present  $s^n$  and next  $s^{n+1}$  grid values for the second order differential is called the Crank-Nicholson scheme [18,19]. This scheme is stable, which means that rapid fluctuations of the grid values that are inevitably introduced by round-off errors are not amplified [18]. The rapid fluctuations would otherwise suppress the important slowly varying part. The following tridiagonal matrix equation has to be solved to obtain the next grid values  $s^{n+1}$  from  $s^n$

$$-ivs_{l+1,m}^{n+1} + (1 + 2iv)s_{l,m}^{n+1} - ivs_{l-1,m}^{n+1} = ivs_{l+1,m}^n + (1 - 2iv)s_{l,m}^n + ivs_{l-1,m}^n, \quad (2.20)$$

where  $v = \Delta z / 4k_s w_z^2 (\Delta \bar{x})^2$ . The equations at the grid boundaries  $l = 0$  and  $l = L$  are

$$-ivs_{1,m}^{n+1} + (1 + iv)s_{0,m}^{n+1} = ivs_{1,m}^n + (1 - iv)s_{0,m}^n \quad \text{and} \quad (2.21)$$

$$(1 + iv)s_{L,m}^{n+1} - ivs_{L-1,m}^{n+1} = (1 - iv)s_{L,m}^n + ivs_{L-1,m}^n. \quad (2.22)$$

The equations (2.20), (2.21), and (2.22) can be written in the following matrix notation with  $s^n = (s_{0,m}^n, s_{1,m}^n, \dots, s_{L,m}^n)$

$$(1 + i\nu H)s^{n+1} = (1 - i\nu H)s^n, \quad (2.23)$$

where  $H$  is an hermitian matrix (i.e.  $H_{ij} = H_{ji}^*$ ). An equation of the form (2.23) is unitary [20] meaning that  $|s^{n+1}| = |s^n|$ . This ensures conservation of power since the power of the Stokes beam is proportional to  $\sum_{l,m} |s_{l,m}^n|^2$ .

The FD method  $U_2$  for the solution of the differential equation  $\partial_z S = \mathcal{L}_2 S$  is obtained by modifying method  $U_1$ . A tridiagonal matrix equation similar to (2.23) can be derived for operator  $\mathcal{L}_2$ , and the method  $U_2$  consists of solving that matrix equation.

The pump field is treated in a similar way as the Stokes field except that  $k_s$  is replaced by  $k_p$ .

#### 2.2.4 The method for the Raman amplification

The amplification of the Stokes beam and the depletion of the pump beam is given by

$$\partial_z S = \frac{g}{2} S |P|^2 \quad \text{and} \quad (2.24)$$

$$\partial_z P = -\frac{g}{2} \frac{k_p}{k_s} P |S|^2. \quad (2.25)$$

These equations can be solved in closed form using the conservation of the (normalized) photon flux [21,22] given by

$$F = |S|^2 + \kappa |P|^2, \quad (2.26)$$

where  $\kappa = k_s/k_p$ . The solution of (2.24) and (2.25) using the constant photon flux (2.26) is

$$\frac{|S(z + \Delta z)|^2}{|P(z + \Delta z)|^2} = \frac{|S(z)|^2}{|P(z)|^2} \exp[g F \Delta z / \kappa]. \quad (2.27)$$

The FD method  $U_3$  for the Stokes and the pump field is based on (2.26) and (2.27). The new values for the Stokes and the pump field on the grid are given by

$$s_{l,m}^{n+1} = s_{l,m}^n \exp[g f_{l,m}^n \Delta z / 2\kappa] \sqrt{\frac{f_{l,m}^n}{\kappa |p_{l,m}^n|^2 + |s_{l,m}^n|^2 \exp[g f_{l,m}^n \Delta z / \kappa]}} \quad (2.28)$$

$$p_{l,m}^{n+1} = p_{l,m}^n \sqrt{\frac{f_{l,m}^n}{\kappa |p_{l,m}^n|^2 + |s_{l,m}^n|^2 \exp[g f_{l,m}^n \Delta z / \kappa]}} \quad (2.29)$$

where

$$f_{l,m}^n = |s_{l,m}^n|^2 + \kappa |p_{l,m}^n|^2. \quad (2.30)$$

## 2.2.5 The method for the grid adjustment

The introduction of the transverse coordinates  $\bar{x}$  and  $\bar{y}$  results in the following differential equation for the Stokes field:

$$\partial_z S = -\frac{1}{2} \left( \partial_z \ln w_z + \partial_z \ln w_y + ik_s \frac{w_{oz}^2 \bar{x}^2}{z_{oz}^2 + (z - z_{fz})^2} + ik_s \frac{w_{oy}^2 \bar{y}^2}{z_{oy}^2 + (z - z_{fy})^2} \right) S. \quad (2.31)$$

This equation can be solved in closed form. The Stokes field at  $z + \Delta z$  is given by

$$S(z + \Delta z) = S(z) \sqrt{\frac{w_z(z) w_y(z)}{w_z(z + \Delta z) w_y(z + \Delta z)}} \times \exp \left[ \frac{ik_s}{2} \left( \frac{w_{oz}^2 \bar{x}^2}{z_{oz}^2} \tan^{-1} \frac{z_{fz} - u}{z_{oz}} + \frac{w_{oy}^2 \bar{y}^2}{z_{oy}^2} \tan^{-1} \frac{z_{fy} - u}{z_{oy}} \right) \right]_{u=s}^{u=s+\Delta s} \quad (2.32)$$

The Stokes field is multiplied by an amplitude factor  $A(z, \Delta z)$  and a phase factor  $\Phi(\bar{x}, \bar{y}, z, \Delta z)$ .

The FD method  $U_4$  for the Stokes field is

$$s_{l,m}^{n+1} = s_{l,m}^n A^n \Phi_{l,m}^n, \quad (2.33)$$

where  $A^n$  and  $\Phi_{l,m}^n$  are based on (2.32). The conservation of energy is ensured by the amplitude factor. The power of the Stokes beam  $P_s^n$  is proportional to  $\sum_{l,m} |s_{l,m}^n|^2 \Delta x \Delta y$ .

Apart from the Raman amplification, the term  $\sum_{l,m} |s_{l,m}^n|^2$  is conserved for all methods  $U_i$ . The amplitude factor in the grid adjustment changes  $\sum_{l,m} |s_{l,m}^n|^2$  to compensate for the change in  $\Delta x \Delta y$ , so that  $P_i^n = P_i^{n+1}$ .

The method for the pump field is obtained by replacing  $k_x$  with  $k_y$  in the phase factor  $\Phi_{l,m}^n$ .

## 2.2.6 Numerical stability and conservation of power

A convenient method of testing the stability of a FD method is the von Neumann stability analysis [18] (or Fourier analysis [19]). If the coefficients of the difference equation are constant (or very slowly varying and to be considered as constants), the independent solutions are of the form

$$u_m^n = \xi^n e^{ik_x m \Delta x}, \quad (2.34)$$

where  $k_x$  is a wavenumber of arbitrary value and  $\xi$  is a complex number depending on  $k_x$ . This  $\xi$  is called the amplification factor at the wavenumber  $k_x$  since  $u_m^{n+1} = \xi u_m^n$ .

Stability of the FD method is determined from  $\xi$  as a function of  $k_x$ . If there is a particular value of  $k_x$  for which  $|\xi(k_x)| > 1$ , then the FD method is called unstable. In principle such an unstable method might be used for small propagation distances if the initial function  $u_m^0$  does not contain the unstable mode(s). However, in practice these unstable modes are high frequency modes (in  $k_x$ ) and these modes are generated by the algorithm through round-off errors. It then depends on the accuracy of the number representation of the computer how many propagation steps can be taken before the erroneous high frequency modes, which grow exponentially with  $|\xi|^n$ , overwhelm the stable low frequency modes. Thus, it is clear that unstable methods should be avoided.

We will now use the von Neumann analysis on the FD method for the diffraction, which we simplify to

$$u_x = i u_{xx} \quad (2.35)$$

Using the Crank-Nicholson scheme, the following FD method is obtained:

$$\frac{u_m^{n+1} - u_m^n}{\Delta x} = i \left( \frac{u_{m+1}^n - 2u_m^n + u_{m-1}^n}{2(\Delta x)^2} + \frac{u_{m+1}^{n+1} - 2u_m^{n+1} + u_{m-1}^{n+1}}{2(\Delta x)^2} \right). \quad (2.36)$$

For the amplification factor  $\xi$ , the following expression is found:

$$\xi = \frac{1 - i \frac{2\Delta z}{(\Delta x)^2} \sin^2 \frac{k_z \Delta x}{2}}{1 + i \frac{2\Delta z}{(\Delta x)^2} \sin^2 \frac{k_z \Delta x}{2}}. \quad (2.37)$$

It is clear that  $|\xi| = 1$  for all values of  $k_z$  and for all  $\Delta x$  and  $\Delta z$ , so the FD method (2.36) is unconditionally stable meaning that the stability does not depend on the step size  $\Delta x$  or the grid size  $\Delta z$ . Furthermore, the method is also unitary because  $|\xi| = 1$  for all  $k_z$ , therefore power is conserved.

In the analysis, we did not consider the influence of boundary conditions on stability. Generally, boundary conditions do not have a drastic influence on stability [16]. In some cases, boundary conditions can just tip the balance and a matrix method should be used [16]. We showed above that the method for the diffraction is unitary for the selected boundary conditions in which case the boundaries operate as perfect mirrors.

Transparent boundaries are sometimes desired, for instance in our simulation of a spurious window reflection in chapter 4. In that particular case, a divergent Stokes beam was amplified by a convergent pump beam and Stokes power had to be removed at the grid boundaries. Intuitively, it can be understood that an extrapolation of the wavefront acts as a transparent boundary

$$u_m^n = cu_{m-1}^n \Rightarrow u_{m+1}^n = cu_m^n \quad (\text{boundary condition}). \quad (2.38)$$

If  $|c| \leq 1$  and  $\text{Im} c > 0$ , then (2.38) represents a transparent boundary. This was independently discovered by Hadley [20], who analyzed this method in some detail. The algorithm is included as an option in the simulation program.

Consistency is another requirement for a FD method. A consistent (or compatible) FD equation converges to the differential equation as  $\Delta x, \Delta z \rightarrow 0$  [16]. This is not trivial as the stable Du Fort-Frankel formula for the differential equation  $u_z = u_{zz}$  shows:

$$\frac{u_m^{n+1} - u_m^{n-1}}{2\Delta z} = \frac{u_{m+1}^n - u_m^{n-1} - u_m^{n+1} + u_{m-1}^n}{(\Delta x)^2}. \quad (2.39)$$

Using the Taylor expansions around  $u_m^n$ , such as

$$u_m^{n+1} = u + \Delta z u_z + \frac{(\Delta z)^2}{2} u_{zz} + O((\Delta z)^3), \quad (2.40)$$

and substituting the expansions in the FD method (2.39), we find

$$u_z = u_{zz} - \frac{(\Delta z)^2}{(\Delta x)^2} u_{zz} + O([\Delta x]^2) + O([\Delta z]^2). \quad (2.41)$$

If  $\Delta z$  and  $\Delta x$  approach 0 with a constant ratio  $\beta = \Delta z/\Delta x$ , the Du Fort-Frankel formula solves the differential equation

$$u_z = u_{zz} - \beta^2 u_{zz}, \quad (2.42)$$

which is not equal to  $u_z = u_{zz}$ ! Thus, the FD method 2.39 solves a different differential equation for each ratio  $\beta = \Delta z/\Delta x$ . Equation 2.41 also provides information on the accuracy of the method; since  $\Delta x$  and  $\Delta z$  appear to the second power in the truncation terms  $O([\Delta x]^2)$  and  $O([\Delta z]^2)$ , the method is called second order accurate in  $x$  and  $z$ .

The Crank-Nicholson scheme for the diffraction equation is both stable and consistent. In addition, it is accurate to second order in  $x$  and  $z$ . For a linear initial value problem, the following theorem holds: [16]

*Equivalence theorem of Lax: Given a properly posed initial boundary value problem and a finite difference approximation to it that satisfies the consistency condition, then stability is the necessary and sufficient condition for convergence.*

Thus the FD method for the diffraction converges to the physical solution. However, there is to our knowledge no mathematical theorem that states that our complete FD method with operator splitting converges to the physical solution.

A fully-explicit FD method has been developed for the diffraction. The above mentioned Crank-Nicholson scheme is an implicit method, since it uses the values at the next time step  $u^{n+1}$  to compute the differential  $u_{zz}$ . An explicit method uses  $u^n$  for all differentials (except of course  $u_z$ ), however, explicit methods often suffer from instability. The following scheme is fully explicit:

$$\begin{aligned} u_m^{n+1/2} &= \frac{i\epsilon}{4}(u_{m-1}^n + u_{m+1}^n) + (1 - \frac{i\epsilon}{2})u_m^n + \frac{i\Delta z}{2(\Delta x)^2}(u_{m+1}^n - 2u_m^n + u_{m-1}^n) \\ u_m^{n+1} &= u_m^n + \frac{i\Delta z}{(\Delta x)^2}(u_{m+1}^{n+1/2} - 2u_m^{n+1/2} + u_{m-1}^{n+1/2}), \end{aligned} \quad (2.43)$$

where  $\epsilon$  is a small number for stabilization of the method and  $u^{n+1/2}$  are intermediate values. Method (2.43) is stable for

$$\epsilon = \frac{1 - 2v^2 - \sqrt{1 - 4v^2}}{2v} \quad \text{and} \quad v = \frac{2\Delta z}{(\Delta x)^2} \leq 0.5. \quad (2.44)$$

For small step sizes, this method is stable and at least twice as fast on the CONVEX C230 as the Crank-Nicholson scheme (for the same step size). However, a serious limitation is the small step size.

### 2.2.7 Accuracy and speed

The accuracy of the method was tested by comparing the FD-propagation of a Gaussian beam with the closed form solution [14]. The Gaussian beam propagated from  $z = -L/2$  to  $z = L/2$  with the focus located at  $z = 0$ . We used the symmetry along the  $x$ - and  $y$ -axis to increase the speed by a factor four. The grid consisted of  $40 \times 40$  points and mapped the first quadrant (because of symmetry).

The accuracy of the FD-method was estimated from the phase shift between  $z = -L/2$  and  $z = L/2$  which is given in closed form by [14]

$$\Delta\phi = 2 \tan^{-1} \frac{L}{2z_0}. \quad (2.45)$$

The FD-method gave  $\Delta\phi = 2.6498$  rad, for  $L/2z_0 = 4$  and a step size of  $\Delta z/2z_0 = 0.04$ ; this  $\Delta\phi$  compared with equation (2.45) gives a relative error of 0.07 %. The propagating beam suffered no power loss which is an advantage over other methods [21].

The speed of the calculation was 30 msec per propagation step. The program ran on a CONVEX C230 and used the vectorization capacity of this computer. The Crank-Nicholson method, which was used for the second order derivatives, is essentially a sequential algorithm. However, the two-dimensional grid made it possible to vectorize the  $\partial_z^2$  differential in the  $y$ -direction and vice versa.

## 2.3 Plane-wave model

For the analysis of the time dependence of the pump and the Stokes pulse, we have developed a plane-wave model that uses one space and one time coordinate without the two transverse

space coordinates. Since the experiments deal with the Stokes energy versus the pump energy, the experimental results are compared with the results of the plane wave model that include the calculated energies of the pump and the Stokes pulse.

The plane wave equations of SRS can be found in many textbooks [1], so we describe these equations briefly. In the forward scattering, the electric Stokes field  $\mathcal{E}_f(z, t)$  is coupled to the electric pump field  $\mathcal{E}_p(z, t)$  through the Raman material vibration  $Q_f(z, t)$ :

$$\frac{1}{v_s} \partial_t \mathcal{E}_f + \partial_z \mathcal{E}_f = iK_2 Q_f^* \mathcal{E}_p, \quad (2.46)$$

$$\frac{1}{v_p} \partial_t \mathcal{E}_p + \partial_z \mathcal{E}_p = iK_3 Q_f \mathcal{E}_f \quad \text{with} \quad K_3 = \frac{v_p k_p}{v_s k_s} K_2, \quad (2.47)$$

$$\partial_t Q_f + \Gamma Q_f = -iK_1 \mathcal{E}_f \mathcal{E}_p^*, \quad (2.48)$$

where  $v_s$  and  $v_p$  are the light speed of the Stokes and the pump field; and  $\Gamma$  is the Raman linewidth (HWHM). Dispersion is not taken into account by the model, so we will use  $v_s = v_p = v$  and  $K_3 = k_p/k_s K_2$ . Backward scattering is described by similar equations, which are obtained by substituting the backward scattered Stokes field  $\mathcal{E}_b(z, t)$  for  $\mathcal{E}_f$ ,  $Q_f(z, t)$  is changed to  $Q_b(z, t)$ , and the  $(1/v \partial_t + \partial_z) \mathcal{E}_f$  differential must be replaced by  $(1/v \partial_t - \partial_z) \mathcal{E}_b$ .

Steady-state approximation of equations (2.46)–(2.48) is often possible, since SRS is a fast process so the material vibration  $Q$  is in equilibrium with the pump and the Stokes field. Under steady-state condition, we find for the material vibration

$$Q_f^* = \frac{-iK_1}{\Gamma} \mathcal{E}_f \mathcal{E}_p^*. \quad (2.49)$$

For the pump and the Stokes field, the following equations are obtained using (2.49):

$$\frac{1}{v} \partial_t \mathcal{E}_f + \partial_z \mathcal{E}_f = \frac{K_1 K_2}{\Gamma} \mathcal{E}_f |\mathcal{E}_p|^2 \quad \text{and} \quad \frac{1}{v} \partial_t \mathcal{E}_p + \partial_z \mathcal{E}_p = -\frac{k_p}{k_s} \frac{K_1 K_2}{\Gamma} \mathcal{E}_p |\mathcal{E}_f|^2. \quad (2.50)$$

These equations can be simplified further by introducing the intensity of the Stokes ( $F$ ) and the pump ( $P$ )

$$F = |\mathcal{E}_f|^2 \quad \text{and} \quad P = |\mathcal{E}_p|^2. \quad (2.51)$$

Note that we use a normalized electric field so that  $|\mathcal{E}|^2$  is equal to the intensity. The equations (2.50) now reduce to

$$\frac{1}{v} \partial_t F + \partial_z F = g F P \quad \text{and} \quad \frac{1}{v} \partial_t P + \partial_z P = -\frac{k_p}{k_s} g F P, \quad (2.52)$$

where  $g$  is the Raman gain coefficient given by  $2K_1K_2/\Gamma$ . Adding the backward scattered Stokes intensity  $B$ , we obtain

$$\frac{1}{v}\partial_t F + \partial_z F = gFP, \quad (2.53)$$

$$\frac{1}{v}\partial_t B + \partial_z B = gBP, \quad (2.54)$$

$$\frac{1}{v}\partial_t P + \partial_z P = -\frac{k_p}{k_s}g(F+B)P. \quad (2.55)$$

The method of characteristics is used to solve the steady-state equations (2.53)–(2.55) as well as the transient gain equations (2.46)–(2.48). We will use the following coordinate transformation (the characteristics):

$$f = vt + z \quad \text{and} \quad b = vt - z. \quad (2.56)$$

It can be shown that equations (2.53)–(2.55) are cast in the following form using  $f$  and  $b$ :

$$\partial_f F = \frac{g}{2}FP, \quad \partial_b B = \frac{g}{2}BP, \quad \text{and} \quad \partial_f P = -\frac{k_p}{k_s}\frac{g}{2}(F+B)P. \quad (2.57)$$

The intensity of the forward Stokes after a propagation step  $\Delta f$  is calculated by

$$F(f + \Delta f, b) = F(f, b)e_F \frac{P(f, b) + F(f, b)}{P(f, b) + F(f, b)e_F} \quad \text{with} \quad e_F = e^{g(F+P)\Delta f/2}. \quad (2.58)$$

Note that this equation is similar to the Raman amplification method in the beam propagation method. An intermediate pump intensity, which is given by

$$P'(f, b) = P(f, b) \frac{P(f, b) + F(f, b)}{P(f, b) + F(f, b)e_F}, \quad (2.59)$$

is used for the calculation of the backward scattered Stokes:

$$B(f, b + \Delta b) = B(f, b)e_B \frac{P'(f, b) + B(f, b)}{P'(f, b) + B(f, b)e_B} \quad \text{with} \quad e_B = e^{g(B+P')\Delta b/2}. \quad (2.60)$$

The pump at  $(f + \Delta f, b)$  is given by

$$P(f + \Delta f, b) = P'(f, b) \frac{P'(f, b) + B(f, b)}{P'(f, b) + B(f, b)e_B}, \quad (2.61)$$

Equations (2.58)–(2.61) can be described by two methods, one for the pump ( $M_p$ ) and the other for the scattered radiation ( $M_s$ ), that are applied sequentially:

$$F(f + \Delta f, b) = M_s(F(f, b), P(f, b)) \quad \text{and} \quad P'(f, b) = M_p(F(f, b), P(f, b)) \quad (2.62)$$

and subsequently

$$B(f, b + \Delta b) = M_s(B(f, b), P'(f, b)) \quad \text{and} \quad P(f + \Delta f, b) = M_p(B(f, b), P'(f, b)). \quad (2.63)$$

By adding similar equations to this chain, other processes such as second Stokes generation can be added to the simulation.

Since the Raman medium is filled with the pump radiation and the scattered radiation over the total length of the medium, the radiation is represented by arrays that give the intensity at a position  $z = m\Delta z$  at a time  $t$ . The pump array  $P_m(t)$  is related to  $P(f, b)$  by

$$P_m(t) = P(f, b) = P(vt + m\Delta z, vt - m\Delta z). \quad (2.64)$$

If  $z$  is advanced by  $\Delta z$ , then  $t$  should be advanced by  $\Delta t = \Delta z/v$  in order to keep the backward coordinate  $b$  constant. Under this condition,  $P(f + \Delta f, b)$  is given by

$$P(f + \Delta f, b) = P_{m+1}(t + \Delta t) \quad \text{with} \quad \Delta f = 2v\Delta t = 2\Delta z. \quad (2.65)$$

The amplification chain (2.62)–(2.63) can now be written in terms of the intensity arrays:

$$F_{m+1}(t + \Delta t) = M_s(F_m(t), P_m(t)) \quad \text{and} \quad P'_m(t) = M_p(F_m(t), P_m(t)), \quad (2.66)$$

and subsequently using  $\Delta b = \Delta f$

$$B_{m-1}(t + \Delta t) = M_s(B_m(t), P'_m(t)) \quad \text{and} \quad P_{m+1}(t) = M_p(B_m(t), P'_m(t)). \quad (2.67)$$

In the transient-gain situation, the notation gets more complicated and the material vibration has to be included in the simulation. However, the principles for the transient-gain simulation are identical to the steady-state situation described above.

We have to modify the plane-wave approximation to the realistic situation of focused beams. In the equations above, the intensity was used, which can be transformed to the power

divided by the beam area  $A$ . The intensity equations (2.53)–(2.55) can now be written in terms of powers and beam area:

$$\frac{1}{v} \partial_t F + \partial_z F = \frac{g}{A} F P = A F P, \quad (2.68)$$

$$\frac{1}{v} \partial_t B + \partial_z B = \frac{g}{A} B P = A B P, \quad (2.69)$$

$$\frac{1}{v} \partial_t P + \partial_z P = -\frac{k_p}{k_s} \frac{g}{A} (F + B) P = -\frac{k_p}{k_s} A (F + B) P. \quad (2.70)$$

using the symbols  $F$ ,  $B$ , and  $P$  for the power instead of the intensity. Focused beams can now be represented by a beam area  $A(z)$  as a function of  $z$ , where  $A(z)$  is given by the area of the undepleted pump. The cross-sectional area of the pump beam is

$$A(z) = \pi w_x(z) w_y(z), \quad (2.71)$$

where  $2w_x$  and  $2w_y$  are the beam diameters in the  $x$ - and  $y$ -direction, referring to the  $1/e^2$  intensity points.

A higher accuracy is obtained by using the amplification obtained from the beam propagation method described in section 2.2. The amplification of the plane wave model is (without pump depletion)

$$\exp\left(\int_{\text{entrance}}^{\text{exit}} A(z) P dz\right). \quad (2.72)$$

By comparing this amplification with the amplification of the beam propagation, which is given by  $(F_{\text{exit}}/F_{\text{entrance}})$ , we can define a gain focusing factor  $\eta$  by

$$\eta = \frac{\ln(F_{\text{exit}}/F_{\text{entrance}})}{\int_{\text{entrance}}^{\text{exit}} A(z) P dz}. \quad (2.73)$$

Gain focusing is the narrowing of the Stokes beam due to the higher amplification at the center of the pump beam. Typical values for  $\eta$  are between 1 and 2. The modified gain coefficient  $A(z)$  is

$$A(z) = \frac{g\eta}{A(z)}. \quad (2.74)$$

Spontaneous noise has to be incorporated in the model for the onset of the scattered radiation. In the equation of the forward Stokes, the spontaneous power  $\delta$  is included as follows

$$\frac{1}{v} \partial_t F + \partial_z F = A(F + \delta) P. \quad (2.75)$$

In the simulation, the spontaneous power is simply added to equations (2.66) and (2.67):

$$F_{m+1}(t + \Delta t) = M_s(F_m(t), P_m(t)) + A(z)\delta P_m(t)\Delta z \quad (2.76)$$

and

$$B_{m-1}(t + \Delta t) = M_s(B_m(t), P'_m(t)) + A(z)\delta P_m(t)\Delta z. \quad (2.77)$$

For the transient gain situation, spontaneous noise is introduced in the material vibration, thus spontaneous scattering is generated indirectly through the material vibration.

Reflections at the windows of the Raman cell have a significant influence on the SRS process. Because of the very high gain ( $e^{25}$  at threshold), a small reflection can still decrease the threshold energy [25]. Furthermore, a dichroic mirror is used to reflect the backward Stokes into the Raman cell so that all Stokes radiation leaves the cell in the forward direction. In the simulation, the reflections can be easily incorporated using

$$F_0(t + \Delta t) = R_{\text{entrance}}B_0(t) \quad (2.78)$$

at the entrance window and

$$B_M(t + \Delta t) = R_{\text{exit}}F_M(t) \quad (2.79)$$

at the exit window. There is no provision for pump reflections in the model.

## 2.4 Results and Discussion

### 2.4.1 Amplification in a spherical lens focus

The FD method that was described above is used to obtain the amplification of a Gaussian Stokes beam by a Gaussian pump beam. The pump beam is focused by an ordinary spherical lens at the middle of the Raman cell of length  $L$ . For the Stokes beam at the entrance window, a width and a divergence that are identical to those of the pump beam are used. The Stokes wave number is identical to the pump wave number in the following calculations. This particular problem has been analyzed by analytical methods and the results of these methods are compared with the results of the FD method.

Table 2.1: Amplification of a Gaussian Stokes beam by a Gaussian pump beam with  $L/2z_o = 4$ .

pump power $\bar{P}_p$	$\ln[\bar{P}_s(L)/\bar{P}_s(0)]$			
	FD method	Kung's method $\frac{1}{2}\bar{P}_p \tan^{-1} \frac{L}{2z_o}$	parabolic pump	matched mode $(\bar{P}_p - 2\sqrt{\bar{P}_p}) \tan^{-1} \frac{L}{2z_o}$
10	7.2	6.6	6.6	4.9
20	16.3	13.3	15.8	14.7
40	37.3	26.5	36.9	36.3
60	59.9	39.8	59.4	59.0

The following expression for the amplification of the Stokes beam has been given by Kung [14,15]

$$\ln \frac{\bar{P}_s(L)}{\bar{P}_s(0)} = \frac{\bar{P}_p}{2} \tan^{-1} \frac{L}{2z_o}, \quad (2.80)$$

where  $\bar{P}_s$  and  $\bar{P}_p$  are the normalized Stokes and the normalized pump power, and  $z_o$  is the Rayleigh range of the pump. Depletion of the pump beam is not considered in (2.80). The following normalization for the Stokes and the pump power is used [6]

$$\bar{P} = g|\mathcal{E}_o|^2 k w_o^2, \quad (2.81)$$

so that  $\bar{P}$  is a dimensionless quantity;  $\mathcal{E}_o$  is the electric field at the focus in the center of the beam, and  $w_o$  is the half width of the beam at the focus. The amplification given by (2.80) for several pump powers is listed in table 2.1 together with the results of the FD method. Comparing the amplifications, we find a higher amplification for the FD method and this difference increases with higher pump power. This higher amplification for the FD method can be explained by considering the narrowing of the Stokes beam due to the higher intensity at the center of the pump beam. The narrowing at high pump powers is called gain focusing [5,6,7].

We shall analyze the gain focusing effect using the approximation that the transverse profile

of the pump beam is represented by a parabola. The Gaussian pump beam is given by

$$|\mathcal{E}_p| = |\mathcal{E}_{p0}| \frac{w_0}{w_p(z)} \exp \left[ -\frac{x^2 + y^2}{w_p^2(z)} \right], \quad (2.82)$$

where  $w_p(z)$  is the half width of the beam. Using the parabolic approximation, the gain profile is given by

$$g|\mathcal{E}_p|^2 \approx g|\mathcal{E}_{p0}|^2 \frac{w_0^2}{w_p^2} \left( 1 - 2 \frac{x^2 + y^2}{w_p^2} \right) = \frac{P_p}{k w_p^2} \left( 1 - 2 \frac{x^2 + y^2}{w_p^2} \right). \quad (2.83)$$

The Stokes beam is given by [6,17]

$$\mathcal{E}_s = \exp \left[ -i \left( \phi(z) + \frac{x^2 + y^2}{2} Q(z) \right) \right], \quad (2.84)$$

where  $\phi(z)$  and  $Q(z)$  are complex functions representing the amplitude and the width of the Stokes beam. The expression for the Stokes beam and the gain profile are substituted in (2.5), the paraxial wave equation, and the terms with the factor  $x^2 + y^2$  are separated from the terms without this factor, which leads to the following set of ordinary differential equations:

$$\partial_z \phi = i \frac{Q}{k} + i \frac{P_p}{2k w_p^2} \quad \text{and} \quad (2.85)$$

$$\partial_z Q = \frac{Q^2}{k} - 2i \frac{P_p}{k w_p^4}. \quad (2.86)$$

These two equations are solved by the Runge-Kutta algorithm.

The amplification given by the parabolic pump model is listed in table 2.1. It is clear from table 2.1 that the values for high pump power correspond very well with the FD method. This can be understood by realizing that the width of the Stokes beam is narrow for high pump power due to the gain narrowing. For a narrow Stokes beam the parabolic approximation is a better approximation than for a wide Stokes beam, and this leads to a better correspondence with the FD method for high pump powers. The effect of gain narrowing on the width of the Stokes beam is shown in figure 2.2. The amplification for low power agrees with the amplification given by (2.80), since for low power the gain narrowing effect is negligible.

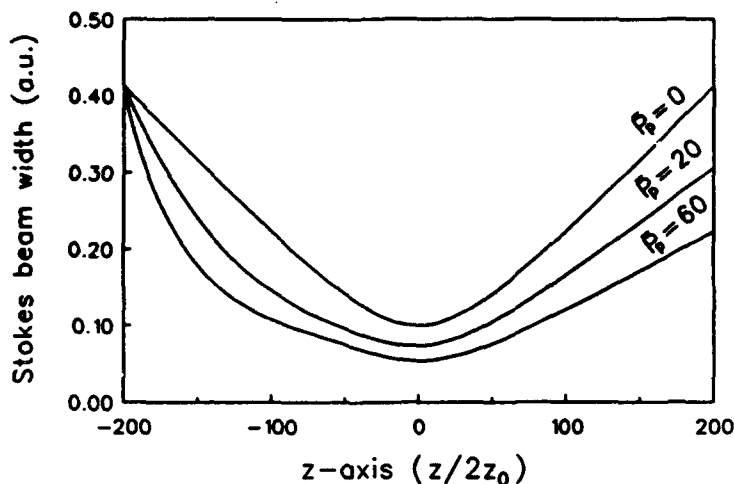


Figure 2.2: Width of the Stokes beam along the  $z$ -axis for several pump powers.

An analytical model for the amplification including gain focusing has been derived by Cotter et al. [6] using the gain focusing formulation of Kogelnik [5] and calculating the amplification of the "matched" Gaussian mode. The matched mode is the mode for which the beam parameters remain constant while propagating through the gain medium [5,6,7]. The amplification of the matched mode is given by [6]

$$\ln \frac{\bar{P}_s(L)}{\bar{P}_s(0)} = (\bar{P}_p - 2\sqrt{\bar{P}_p}) \tan^{-1} \frac{L}{2z_0}, \quad (2.87)$$

In table 2.1 the results of (2.87) for several pump powers are shown. The results of (2.87) correspond very well with the FD method for high pump powers.

#### 2.4.2 Amplification in an astigmatic focus

We shall use the FD method to obtain the amplification of an elliptic Gaussian Stokes beam by an elliptic Gaussian pump beam. The pump beam is focused by an astigmatic lens or by a pair of cylindrical lenses at the middle of the Raman cell. The astigmatic focus of a Gaussian beam is characterized by (2.7) and (2.8), where  $z_{fx}$  and  $z_{fy}$  are the place of the foci in the  $x$ - $z$  and the  $y$ - $z$  plane, respectively. An important parameter describing the astigmatic focus is the distance  $\Delta F$  between the two foci, which is  $|z_{fx} - z_{fy}|$ . Figure 2.3

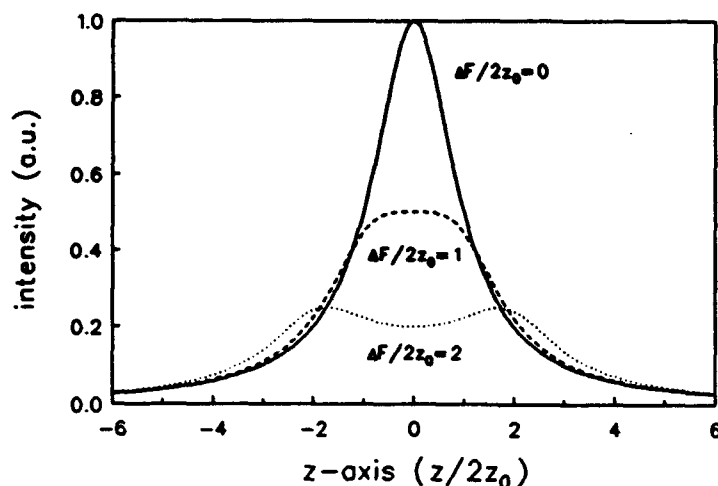


Figure 2.3: Intensity on the optical axis for several values of  $\Delta F$ .

shows for several values of  $\Delta F$  the intensity of the pump beam on the optical axis given by [17]

$$I_p(x=0, y=0, z) = I_0 \frac{w_{0x} w_{0y}}{w_x(z) w_y(z)}, \quad (2.88)$$

where  $I_0$  is a constant;  $w_x$  and  $w_y$  are given by (2.7) and (2.8). It is clear that the intensity profile is strongly influenced by  $\Delta F$ .

The amplification of the Stokes beam versus  $\Delta F$  is shown in figure 2.4. Obviously, the amplification decreases for increasing  $\Delta F$ . This decrease of the amplification is caused by a decrease of the intensity in the focal region. In figure 2.5 the intensity at the focus in the center of the beam versus  $\Delta F$  is shown, and it is clear that the intensity drops rapidly as  $\Delta F$  is increased.

At high light intensity, Raman media are transformed into a high absorbing plasma. This transition into the opaque state is called optical breakdown [26,27]. This breakdown effect has to be suppressed in an efficient Raman cell. Therefore, the power of the pump beam is limited so that the intensity at the focus does not exceed the breakdown threshold. However, decreasing the power of the pump beam will also reduce the amplification of the Stokes beam.

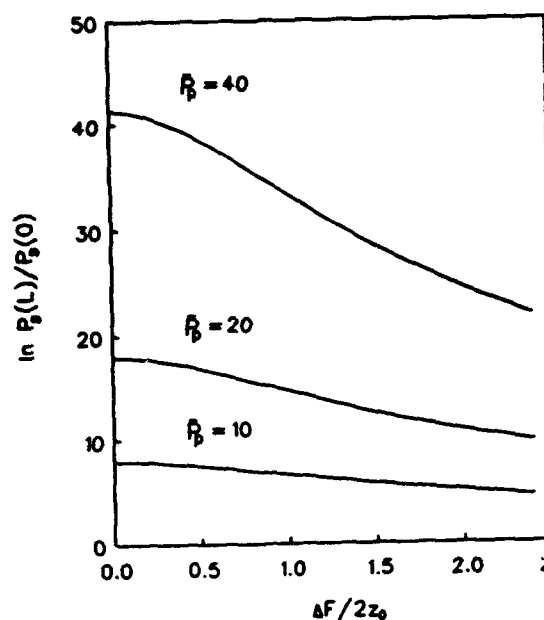


Figure 2.4: Amplification of the Stokes beam versus  $\Delta F$  for several pump powers. The following parameters are used:  $z_o = z_{ox} = z_{oy}$ ,  $k_s = k_p$ , and  $L/2z_o = 10$ .

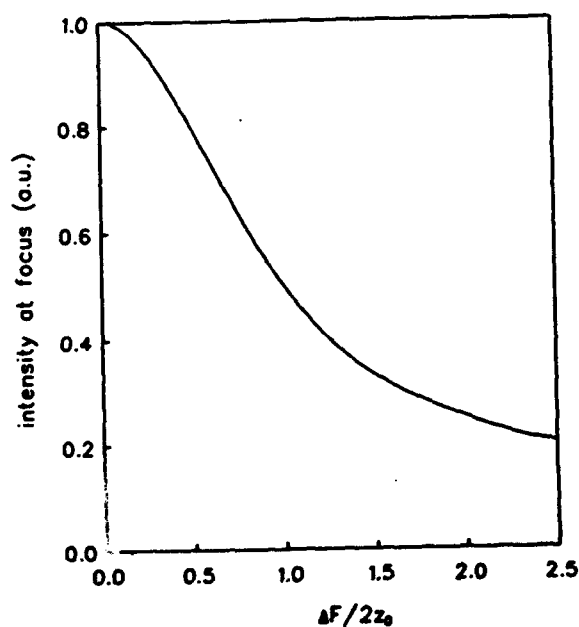


Figure 2.5: Intensity at the focus in the center of the pump beam versus  $\Delta F$ .

Astigmatic lenses can be used to reduce the intensity in the focus and thus eliminating optical breakdown without increasing the length of the Raman cell. As figure 2.5 shows, the intensity in the focus drops rapidly with increasing  $\Delta F$ ; a  $\Delta F$  equal to the confocal parameter  $2z_0$  reduces the intensity with a factor 2. Figure 2.4 shows that the amplification is reduced only slightly with a factor 1.2 for  $\Delta F = 2z_0$ . Thus, an astigmatic lens gives approximately the same amplification as a spherical lens, but with a lower intensity at the focus.

For a high energy pump beam in combination with a tight focus, the conversion to a high energy Stokes beam is limited by the number of atoms or molecules in the ground state [1,22]. This saturation effect is called ground-state depletion and occurs when the relaxation time of the final Raman level is long compared to the pulse width of the laser. Under these conditions the number of generated Stokes photons is limited by the number of atoms (or molecules) in the volume where the conversion takes place, i.e. the focal region. We calculate the volume of the focal region using the area of the cross-section of the elliptic Gaussian beam and the length of the focal region:

$$V = \int_{z_1}^{z_2} \pi w_z(z) w_y(z) dz, \quad (2.89)$$

where  $w_z$  and  $w_y$  are the widths of the beam given by (2.7) and (2.8);  $z_1$  and  $z_2$  are the positions on the optical axis where the intensity is half the maximum intensity. Figure 2.6 shows the volume given by (2.89) as a function of  $\Delta F$ . It is clear that the volume increases rapidly with  $\Delta F$ ; for  $\Delta F = 2z_0$  the volume is about a factor 3 larger compared to  $\Delta F = 0$ . This means that the energy of a Stokes beam limited by ground-state depletion can increase substantially by using an astigmatic focus. However, chapter 5 shows that ground-state depletion is negligible in our experimental setup. Furthermore, simulations show that the effective volume is significantly larger than the volume given by (2.89).

In a Raman cell with spherical lenses, the intensity at the focus can be reduced and the volume of the focal region can be increased by the use of a longer focal length. However, this approach has the disadvantage that it results in an unwieldy long Raman cell. Furthermore, the length of a Raman cell is not as easily adjusted as the distance between two cylindrical lenses (changing  $\Delta F$ ). Another advantage of a short Raman cell with an astigmatic focus is related to the gain enhancement by a dichroic mirror at the entrance window. The function of such a dichroic mirror is to reflect the backward scattered Stokes beam back into the cell while not affecting the pump beam [14,28]. A short Raman cell is essential for this method of gain enhancement since the delay of the reflected Stokes pulse must be short in order to

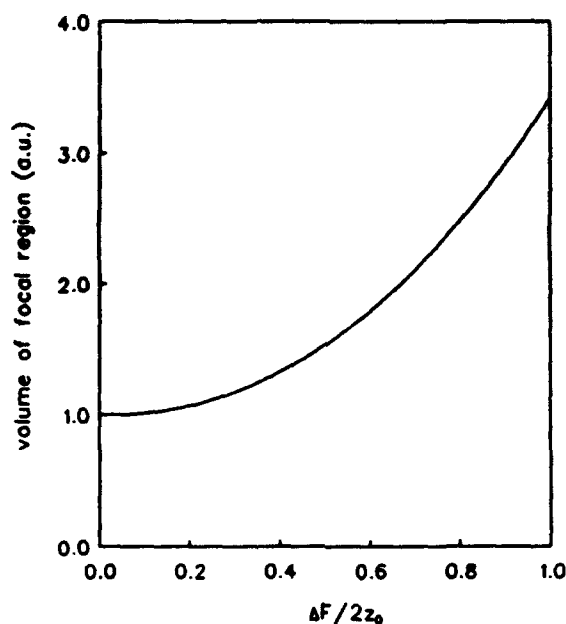


Figure 2.6: Volume of the focal region versus  $\Delta F$ .

overlap with the pump beam.

## 2.5 Summary and Conclusions

A three-dimensional finite difference method has been presented for the propagation of beams focused by an astigmatic lens. This FD method is stable and unitary, which means that the power of the beams is conserved.

The FD method is used for the modeling of a Raman amplifier. The results of the FD method have been cross-checked with analytical models and with a numerical model that describes gain focusing. It has been shown that the FD method gives reliable results both for low and for high pump power.

At high light intensity, optical breakdown occurs and this effect can limit the efficiency of a Raman cell. It has been shown that astigmatic lenses lessen the problem of optical breakdown by reducing the intensity at the focus while maintaining sufficient gain.

### 3 EXPERIMENTS USING METHANE

#### 3.1 Experimental setup

A diagram of the experimental setup is shown in fig. 3.1. A Q-switched Nd:YAG laser was used to generate the pump beam. The BMI-501-D.NS laser provided  $1.06\text{ }\mu\text{m}$  pulses up to 350 mJ in energy with a FWHM pulse width of 7 ns. Using a fast photo detector with a rise and fall time of 1 ns, we measured the pump power. The pump pulses showed some beating as can be seen from the 1 GHz oscilloscope trace shown in fig. 3.2. Beating at 300 MHz can be attributed to the longitudinal mode spacing of the 50 cm long laser resonator. A circular diaphragm could be placed inside the laser cavity to control the quality of the beam. We used two diaphragm sizes in our experiments, namely a diameter of 1.5 mm and a diameter of 6.5 mm. The beam quality, i.e. the  $M^2$  factor, was measured using a standard knife-edge technique; details of the  $M^2$  measurement are described in section 3.3. The energy of the laser beam was adjusted by an attenuator before the beam entered the Raman cell.

The pump beam was focused into the Raman cell by an ordinary spherical lens of 10 cm focal length or by a pair of cylindrical lenses of 10 cm focal length placed 1.3 cm apart. At the entrance of the Raman cell a dichroic mirror was placed to reflect the backward scattered Stokes into the Raman cell in order to obtain all Stokes radiation in the forward direction. For the threshold measurements of chapter 4, we did not use the dichroic mirror and we only used the spherical lens.

The 20 cm long Raman cell contained methane with a pressure of 88 bar. A window was mounted on top of the cell so that visible sparking due to, unwanted, optical breakdown could be observed. To avoid optical breakdown, we measured upto 200 mJ for the ordinary focus; for the astigmatic focus we measured upto 250 mJ. No sparking was observed below these energies.

Calibrated pyroelectric detectors were used to measure the pulse energies of the pump pulse and the generated pulses. Various filters at the exit window (selective mirrors, color glass filters) were used to select and measure the first Stokes, the second Stokes, or the anti-Stokes. The energy of the initial pump beam was measured with a second detector using the reflection of the beam sampler. Brillouin scattering was measured by monitoring the backward scattered  $1.06\text{ }\mu\text{m}$  beam.

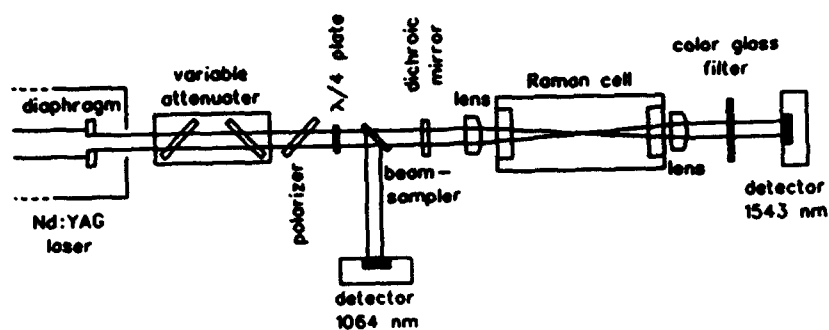


Figure 3.1: Experimental setup.

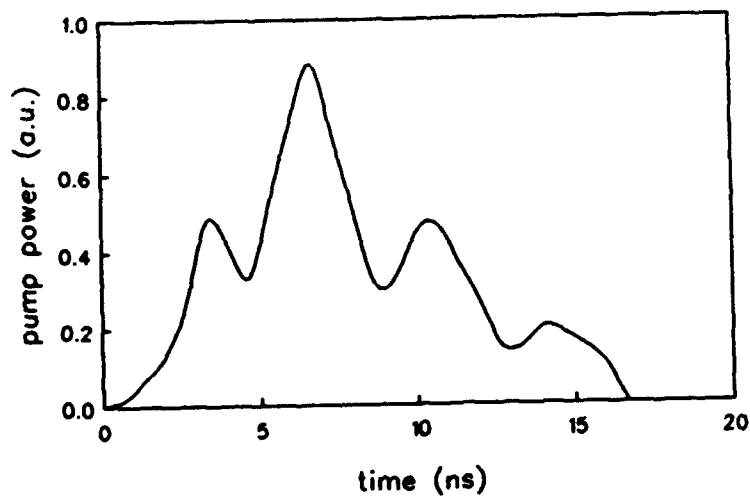


Figure 3.2: Digitized oscilloscope trace of the pump pulse.

### 3.2 Methane parameters

For our simulations, the Raman gain coefficient has to be obtained. The expression for the gain of SRS is given by [26]

$$g = \frac{2\lambda_s^2 \Delta N}{h\nu_s \pi \Delta\nu} \cdot \left( \frac{\partial\sigma}{\partial\Omega} \right), \quad (3.1)$$

where  $\lambda_s$  is the Stokes wavelength in the medium;  $h\nu_s$  is the energy of the Stokes photon;  $\Delta N$  is the population difference between the initial and final states;  $\Delta\nu$  is the linewidth (FWHM); and  $(\partial\sigma/\partial\Omega)$  is the differential scattering cross section in intensity ratio. Since these quantities depend on the pump wavelength and on the gas pressure, the Raman gain coefficient is calculated using the following relations:

- $(\partial\sigma/\partial\Omega)$  as a function of pump wavelength.
- dependence of  $\Delta\nu$  on gas pressure.
- refractive index  $n_s$  versus gas pressure.
- molecular density  $N_{\text{tot}}$  as a function of gas pressure.

The differential scattering cross section is described by [27]

$$\left( \frac{\partial\sigma}{\partial\Omega} \right)_{\nu_s} = \left[ \left( \frac{\partial\sigma}{\partial\Omega} \right)_{\nu'_s, N_2} (\nu'_s)^{-4} \right] \nu_s^4 C(\nu_p, \nu'_p) \Sigma(\nu'_p), \quad (3.2)$$

where  $(\partial\sigma/\partial\Omega)_{\nu'_s, N_2}$  is the differential scattering cross section of nitrogen at  $\nu'_p$ ;  $\nu_p$  and  $\nu_s$  stand for the pump and the Stokes frequency;  $C(\nu_p, \nu'_p)$  is a correction factor to account for the difference in the tabulated and the required pump frequency; and  $\Sigma(\nu'_p)$  is the tabulated relative cross section given by Schrötter and Klöckner [28]. Since there is no clear wavelength dependence of  $\Sigma(\nu'_p)$  for methane, we will use the average value 8.56 for  $\Sigma$  (and no correction factor). At the pump wavelength of 1.06  $\mu\text{m}$ , a  $(\partial\sigma/\partial\Omega)$  of  $7.6 \times 10^{-32} \text{ cm}^2/\text{sr}$  is obtained using  $[(\partial\sigma/\partial\Omega)_{N_2}(\nu'_s)^{-4}] = 5.05 \times 10^{-48} \text{ cm}^6/\text{sr}$ , which is constant for all  $\nu'_s$ . The accuracy of  $(\partial\sigma/\partial\Omega)$  is around 10%, which makes it the quantity with the lowest accuracy [26].

According to Ottusch and Rockwell [26], the linewidth as a function of the gas pressure is

$$\Delta\nu = 8.4 \times 10^9 + 3.9 \times 10^8 p \quad [\text{Hz}] \quad \text{with } p \text{ in } [\text{atm}]. \quad (3.3)$$

So for 88 bar, we obtain a linewidth of 42.7 GHz.

For the refractive index of methane versus the gas pressure, we find [29]

$$n_s = 1 + 4.44 \times 10^{-4} p \quad \text{with } p \text{ in [atm]}. \quad (3.4)$$

In the calculation of the molecular density of methane, nonideality of the gas is accounted for by using the following expression:

$$\left(p + \frac{n^2 a}{V^2}\right)(V - nb) = nRT, \quad (3.5)$$

where  $n$  is the number of moles,  $R$  is the gas constant, and  $T$  is the absolute temperature. For methane, the constants  $a$  and  $b$  are [29]

$$a = 2.253 \times 10^6 \text{ cm}^6 \text{ atm/mol}^2 \quad \text{and} \quad b = 42.78 \text{ cm}^3/\text{mol}. \quad (3.6)$$

At a pressure of 88 bar, a density  $N_{\text{tot}}$  of  $5.53 \times 10^{21} \text{ cm}^{-3}$  is found. For methane, we have  $\Delta N = N_{\text{tot}}$  (cf.  $\Delta N = 0.66 N_{\text{tot}}$  for hydrogen).

Using these values, we obtain a gain coefficient of 0.49 cm/GW for a pump wavelength of 1.06  $\mu\text{m}$  and a gain coefficient of 0.27 cm/GW for the second Stokes generation. Equation (3.1) shows that the gain coefficient is proportional to  $1/\nu_s$ , since  $(\partial\sigma/\partial\Omega)$  is proportional to  $\nu_s^4$ . The relation between the gain and the gas pressure is depicted in figure 3.3 showing a saturation at high pressures due to the increase of the linewidth.

An estimation of the spontaneous Raman noise is made using the spontaneous intensity  $\Gamma\hbar\omega_s/4A$  as derived in [30]. A noise power  $\delta$  of  $10^{-9}$  W is obtained in this way. Correcting for the higher divergence of the pump beam with  $M^2 = 8.7$ , we obtain a noise power  $\delta$  of  $M^4 \times 10^{-9}$  W, i.e.  $10^{-7}$  W.

### 3.3 Beam quality measurements

The beam quality (i.e. the  $M^2$  factor) was measured using a standard knife-edge technique. A lens with a 75 cm focal length was placed in the pump beam, and the width of the beam at various distances from the lens was measured with the knife-edge technique. We used

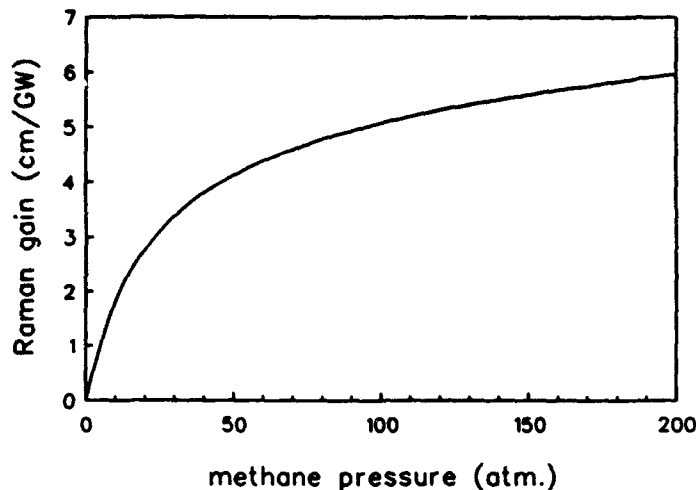


Figure 3.3: Raman gain coefficient of methane versus gas pressure for a pump wavelength of  $1.06 \mu\text{m}$ .

the clip levels of 10% and 90%, as discussed by Siegman in ref. [31], to obtain the beam radius  $w(z)$  using

$$w = 0.78D_c, \quad (3.7)$$

where  $D_c$  is the clip width, i.e. the separation of the 10% and the 90% cut-off levels. We also used the clip levels of 16% and 84% using the following expression:

$$w = 1.0D'_c, \quad (3.8)$$

with  $D'_c$  as the new clip width. The difference for these two methods was typically 5%. Figure 3.4 shows the measured beam radius versus the knife position as well as the theoretical relation

$$w^2(z) = w_0^2 \left( 1 + \frac{(z - z_0)^2}{z_R^2} \right) \quad \text{with} \quad z_R = \frac{kw_0^2}{2M^2}. \quad (3.9)$$

This expression for the Rayleigh range  $z_R$  was used to obtain the  $M^2$  factor. For the 1.5 mm diaphragm, an  $M^2$  factor of  $1.12 \pm 0.05$  was found. Since this  $M^2$  value is close to one, the beam for the 1.5 mm diaphragm is almost diffraction-limited. A much higher  $M^2$  value was found for the 6.5 mm diaphragm, namely  $8.7 \pm 0.3$ .

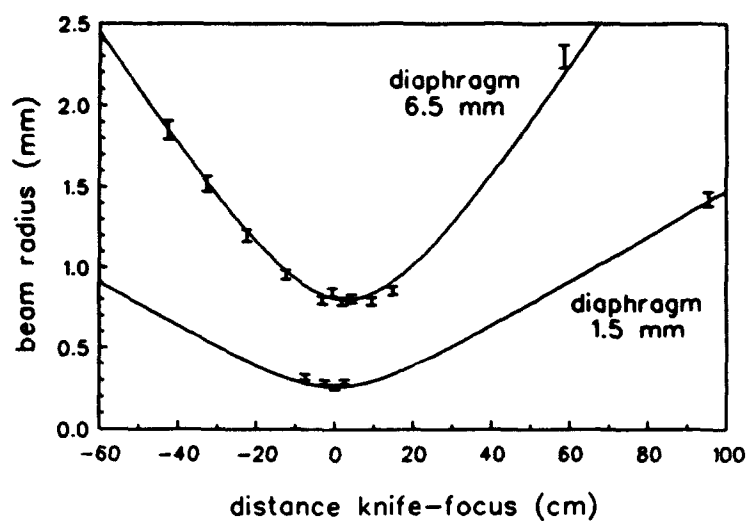


Figure 3.4: Beam radius versus distance from focus. The lines indicate the theoretical relation for  $M^2 = 1.12$  and  $M^2 = 8.7$ .

A pyroelectric matrix array of  $32 \times 32$  elements was used to measure the pump beam profile. Figure 3.5 shows the near-field profile of the pump beam for the 6.5 mm diaphragm. It is clear that the profile is approximately Gaussian; i.e. there are no sharp peaks due to higher order modes.

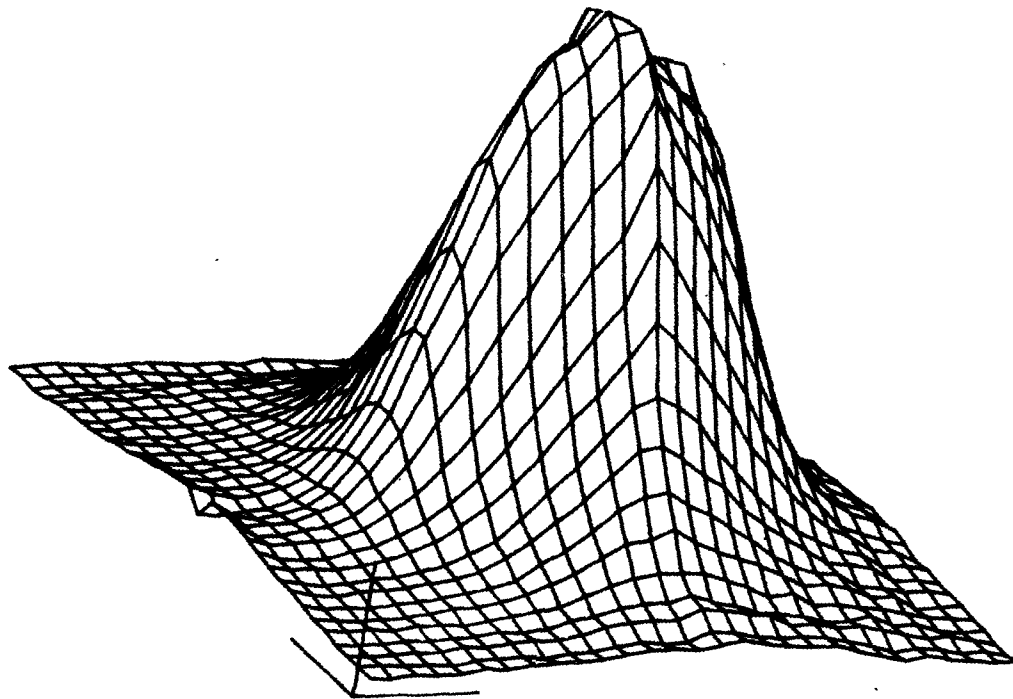


Figure 3.5: Measured beam profile of the 1.06 μm pump beam for a laser diaphragm of 6.5 mm diameter.

## 4 THRESHOLD OF STIMULATED RAMAN SCATTERING

### 4.1 Introduction

In this chapter we study the effect of pump beam quality on the threshold power. The SRS process has no real threshold like a laser, but an experimental threshold can be defined. Here the threshold stands for the pump power corresponding to 1 percent conversion efficiency. By changing the diaphragm inside the laser, we could change the quality of the output beam. Because the original laser beam (called the pump beam) is focused into the Raman medium, the SRS process will depend on the beam quality since the process is driven by the intensity at the focus. We present theoretical and experimental results for a nondiffraction-limited pump beam.

The beam quality is related to the  $M^2$  factor which is a dimensionless factor that compares the divergence of a given beam with the divergence of a (diffraction-limited) Gaussian beam. The divergence of an arbitrary beam can be defined unambiguously using the variances  $\sigma_x^2$  and  $\sigma_y^2$  of the beam profile in the two transverse directions. It has been shown that these variances  $\sigma_x^2$  and  $\sigma_y^2$  increase proportionally to the square of the distance from the waist, i.e. where the width is smallest, which is similar to the width change of Gaussian beams [32,31]. By comparing the rate of increase of the variance of an arbitrary beam (i.e. the divergence) with the corresponding rate of a Gaussian beam with the same waist width, the  $M^2$  factor can be determined. This  $M^2$  factor is a fundamental property of the beam which is not changed by a lens if the lens has a sufficient diameter to avoid truncation of the beam profile and negligible spherical aberration [8]. In fact, the  $M^2$  determines the intensity at the lens focus and the length of the focus; the product of these quantities is a factor  $1/M^2$  lower compared to a TEM<sub>00</sub> beam.

The amplification of a Raman shifted beam (i.e. the Stokes beam) by a nondiffraction-limited pump beam is solved numerically. A finite difference (FD) method is used for this problem of beam propagation in a gain medium that is generated by the pump beam. The details of the FD method have been reported in ref. [33]. For the nondiffraction-limited pump beam, Gaussian-Hermite (G-H) beams, Gaussian-Laguerre (G-L) beams, and Gaussian-Schell-model (GSM) beams are used. The  $M^2$  factor of these beams can be calculated analytically. A random superposition of G-H modes is also used as a pump beam; for this type of beam, the  $M^2$  factor is obtained numerically.

Experiments were performed to confirm the relation between threshold and beam quality. A Nd:YAG laser beam was focused into a Raman cell containing high pressure methane as the Raman medium. The pump beam quality was varied by changing the diaphragm inside the Nd:YAG laser cavity. Subsequently, the Stokes energy was measured as a function of pump energy. We compared the experimental Stokes energy with the simulated Stokes energy for low pump energies. A good agreement was found both for high ( $M^2 = 1.12$ ) and low ( $M^2 = 8.7$ ) beam quality.

## 4.2 Theory

### 4.2.1 The beam propagation method

In the paraxial approximation the propagation of the Stokes field  $\mathcal{E}_s$  and the pump field  $\mathcal{E}_p$  is given by [6,13]

$$\partial_z^2 \mathcal{E}_s + \partial_y^2 \mathcal{E}_s + 2ik_s \partial_z \mathcal{E}_s = ik_s g \mathcal{E}_s |\mathcal{E}_p|^2 \quad \text{and} \quad (4.1)$$

$$\partial_z^2 \mathcal{E}_p + \partial_y^2 \mathcal{E}_p + 2ik_p \partial_z \mathcal{E}_p = -i \frac{k_p^2}{k_s} g \mathcal{E}_p |\mathcal{E}_s|^2, \quad (4.2)$$

where  $k_s$  and  $k_p$  are the wave numbers of the Stokes and the pump field and  $g$  is the Raman gain coefficient. These two partial differential equations can be considered as an initial value problem with the space coordinate  $z$  instead of the time coordinate. The spontaneous Stokes is incorporated by using an initial seed beam which is amplified by the gain medium generated by the pump beam. A finite difference (FD) method is used to solve (4.1) and (4.2) by numerically integrating these equations along the  $z$ -axis; the details of the method have been reported in chapter 2.

A two-dimensional grid is used by the FD method to contain the beam profiles. In this way it is possible to study the propagation of Gaussian-Hermite (G-H) and Gaussian-Laguerre (G-L) beams which are not radially symmetric. The field of the G-H TEM<sub>mn</sub> mode, without phase component, is given by [34]

$$\mathcal{E}_{mn}(x, y, z) = \frac{\mathcal{E}_0}{w(z)} H_m \left( \frac{\sqrt{2} x}{w(z)} \right) H_n \left( \frac{\sqrt{2} y}{w(z)} \right) \exp \left( -\frac{x^2 + y^2}{w^2(z)} \right), \quad (4.3)$$

where  $\mathcal{E}_0$  is an amplitude factor;  $H_n(x)$  is the Hermite polynomial of the order  $n$ ; and  $w(z)$  is the beam radius of the corresponding fundamental Gaussian beam. The G-L TEM<sub>pl</sub> modes are of the form [34]

$$\mathcal{E}_{pl}(r, \phi, z) = \frac{\mathcal{E}_0}{w(z)} \left( \frac{\sqrt{2} r}{w(z)} \right)^\ell L_p^\ell \left( \frac{2r^2}{w^2(z)} \right) \cos \ell \phi \exp \left( \frac{-r^2}{w^2(z)} \right), \quad (4.4)$$

where  $L_p^\ell(x)$  is the Laguerre polynomial.

The  $M^2$  factor of the G-H and the G-L modes can be calculated from the variances  $\sigma_x^2$  and  $\sigma_y^2$  given by [32]

$$\sigma_x^2 = \frac{1}{N} \iint (x - \bar{x})^2 I(x, y) dx dy \quad \text{and} \quad (4.5)$$

$$\sigma_y^2 = \frac{1}{N} \iint (y - \bar{y})^2 I(x, y) dx dy, \quad (4.6)$$

where  $I(x, y)$  is the intensity of the beam profile;  $\bar{x}$  and  $\bar{y}$  are averages defined as

$$\bar{x} = \frac{1}{N} \iint x I(x, y) dx dy \quad \text{and} \quad \bar{y} = \frac{1}{N} \iint y I(x, y) dx dy; \quad (4.7)$$

and  $N$  is the normalization factor given by

$$N = \iint I(x, y) dx dy. \quad (4.8)$$

These integrals can be solved analytically. For the G-H modes the variances are

$$\sigma_x^2 = w^2(1 + 2m)/4 \quad \text{and} \quad \sigma_y^2 = w^2(1 + 2n)/4. \quad (4.9)$$

The variances of the G-L modes for  $\ell \neq 1$  are

$$\sigma_x^2 = \sigma_y^2 = w^2(1 + 2p + \ell)/4; \quad (4.10)$$

for  $\ell = 1$  the variances are

$$\sigma_x^2 = 3w^2(1 + p)/4 \quad \text{and} \quad \sigma_y^2 = w^2(1 + p)/4. \quad (4.11)$$

By comparing the rate of change of the variances with the rate for a TEM<sub>00</sub> beam, the  $M^2$  factor is obtained. This gives

$$M_x^2 = \frac{4\sigma_x^2}{w^2} \quad \text{and} \quad M_y^2 = \frac{4\sigma_y^2}{w^2}. \quad (4.12)$$

We shall combine  $M_x^2$  and  $M_y^2$  to obtain  $M^2$  using

$$M^2 = M_x M_y. \quad (4.13)$$

With this definition,  $M^2$  is defined for elliptical beams and  $M^2$  is not changed by astigmatic lenses.

The Gaussian-Schell-model (GSM) beam has a Gaussian intensity profile given by [35]

$$I(r, z) = \frac{I_0}{w^2(z)} \exp\left(\frac{-2r^2}{w^2(z)}\right), \quad (4.14)$$

which is identical to a fundamental Gaussian beam. However, the width in (4.14) differs from the fundamental beam and is of the form [36]

$$w^2(z) = w_0^2 \left(1 + \frac{(z - z_0)^2}{z_R^2}\right) \quad \text{with} \quad z_R = \frac{kw_0^2}{2M^2}, \quad (4.15)$$

where  $w_0$  is the beam radius at the waist,  $z_0$  is the position of the waist, and  $z_R$  is the Rayleigh range. Equation (4.15) shows that the Rayleigh range for the GSM beam is reduced by the beam quality factor  $M^2$ .

#### 4.2.2 Time dependence

In order to compare the experimental results with the numerical model, the time dependence of the pump pulse has to be taken into account. The reason for this is that the experimental set-up measures the pulse energy of the Stokes and the pump pulse and not the power. To reduce the complexity, the power of the Stokes and the pump beam are used instead of the full beam profile. In this way the following equations are obtained [1]

$$\frac{n}{c} \partial_t F + \partial_z F = A(z) F P, \quad (4.16)$$

$$\frac{n}{c} \partial_t B - \partial_z B = A(z) B P, \quad (4.17)$$

$$\frac{n}{c} \partial_t P + \partial_z P = -\frac{k_p}{k_s} A(z) (F + B) P, \quad (4.18)$$

where  $P(z, t)$ ,  $F(z, t)$ , and  $B(z, t)$  are the pump power, the forward scattered Stokes power, and the backward scattered Stokes power, respectively;  $c/n$  is the speed of light in the medium. The gain parameter  $A(z)$  is obtained from the beam propagation method, described above, using the peak power of the pump pulse. To solve eqns. (4.16)–(4.18), the method of characteristics is used. The numerical method is described in chapter 2.

An experimental complication is the small but significant reflection at the windows of the Raman cell. Because of the very high gain ( $e^{25}$  at threshold), a small reflection can still decrease the threshold energy [22]. Therefore, the input parameters include the reflection coefficient at the windows.

#### 4.3 Results and Discussion

##### 4.3.1 Numerical results of the beam propagation method

We use the beam propagation method of section 4.2 to determine the amplification of a Stokes beam by a nondiffraction-limited pump beam. For the initial Stokes beam, a  $TEM_{00}$  beam is used. For the pump beam, different shapes are used, namely, Gaussian-Hermite (G-H) modes, Gaussian-Laguerre (G-L) modes, and Gaussian-Schell-model (GSM) beams. The various pump profiles are given by eqns. (4.3) and (4.4), where  $w(z)$  is the beam radius of the free space Stokes beam; the waist location of the pump and Stokes beam is at the middle of the Raman cell.

Figure 4.1 shows the amplification of the Stokes beam versus pump power for various pump shapes with  $M^2$  factors of 1, 1.73, 3, and 5. It is clear that the amplifications near the threshold level ( $e^{25}$ ) are nearly equal for beams with different shapes but an identical  $M^2$  factor. For instance, the G-H  $TEM_{01}$  mode, with an  $M^2$  given by (4.13)

$$M^2 = M_x M_y = \sqrt{1+2m} \sqrt{1+2n} \Rightarrow M^2 = \sqrt{3} \approx 1.73, \quad (4.19)$$

has a threshold power ( $\approx 2$  a.u.) almost identical to the GSM beam with the same  $M^2$ .

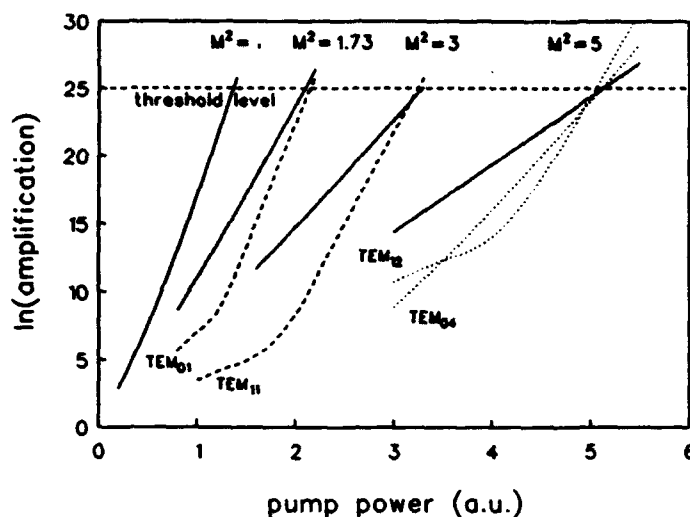


Figure 4.1: Amplification of the Stokes beam versus pump power for various pump beams. The solid lines indicate the GSM beams, the dashed lines indicate the G-H  $TEM_{mn}$  beams, and the dotted lines indicate the G-L  $TEM_{p\ell}$  beams.

By examining the Stokes beam profile, we see that at the threshold level the Stokes beam profile reproduces to a certain extent the shape of the pump beam. This is illustrated in fig. 4.2 for a G-H  $TEM_{01}$  pump beam of sufficient power so that the amplification is at the threshold level. It is clear from the figure that the Stokes profile shows the two maxima of the pump profile. At low pump power, the diffraction dominates over the amplification so that the Stokes beam does not reproduce the pump beam. This is illustrated in fig. 4.3, where there is only a small stretching due to the amplification.

The relation between the threshold power and the  $M^2$  factor is, unfortunately, not always so close as for the pump shapes of fig. 4.1. In particular, the circular symmetric G-L  $TEM_{10}$  mode shows a large difference in amplification compared to the GSM beam. This is shown in fig. 4.4 for the G-L  $TEM_{10}$  pump beam ( $p = 1$  and  $\ell = 0$ ) with  $M^2 = 3$ . Figure 4.4 shows a much higher amplification for the  $TEM_{10}$  beam compared to the GSM beam, which results in a threshold power that is about 40% lower than that of the GSM beam.

The Stokes beam profile for a high power G-L  $TEM_{10}$  pump beam is shown in fig. 4.5. It is clear that the Stokes beam profile does not reproduce that of the pump beam. The center of the pump profile is much higher than the surrounding ring so that the amplification is mainly at the center. This particular profile combines a high beam radius due to the ring

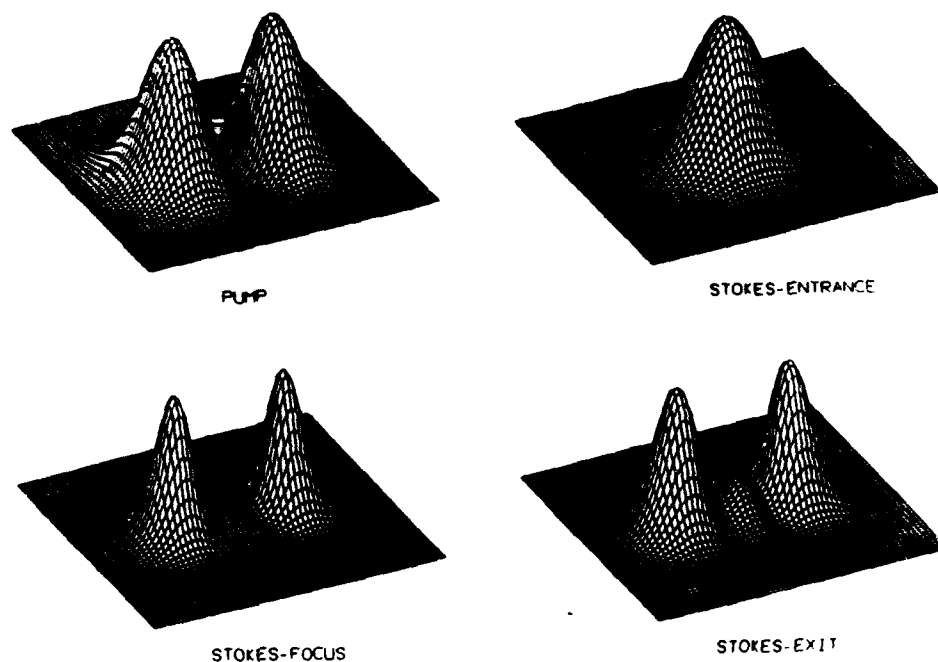


Figure 4.2: Beam profiles, for high pump power, of the G-H  $TEM_{01}$  pump beam and of the Stokes beam at the entrance, middle, and exit of the Raman cell.

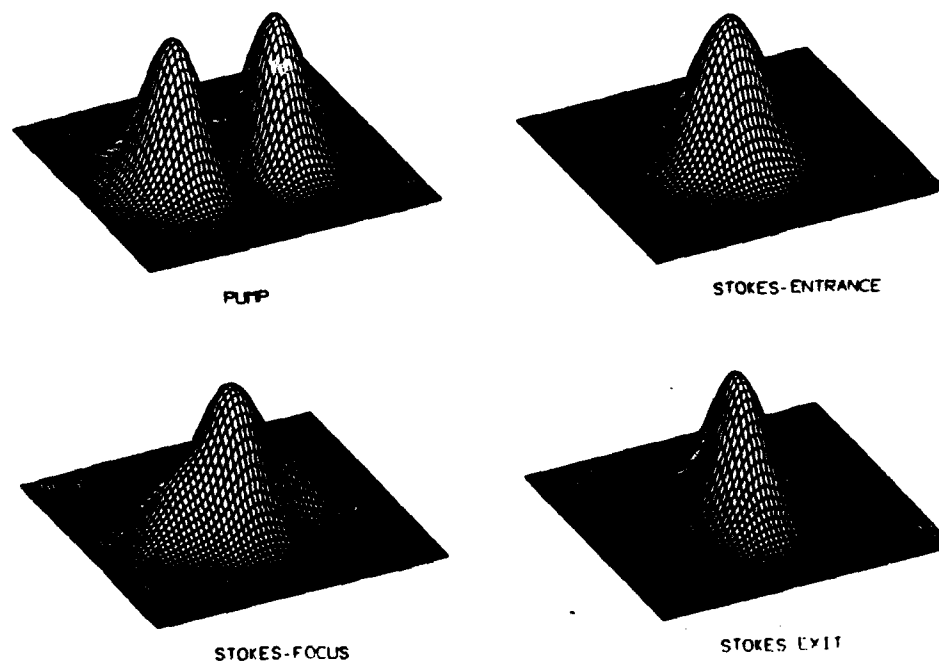


Figure 4.3: Beam profiles, for low pump power, of the G-H  $TEM_{01}$  pump beam and of the Stokes beam at the entrance, middle, and exit of the Raman cell.

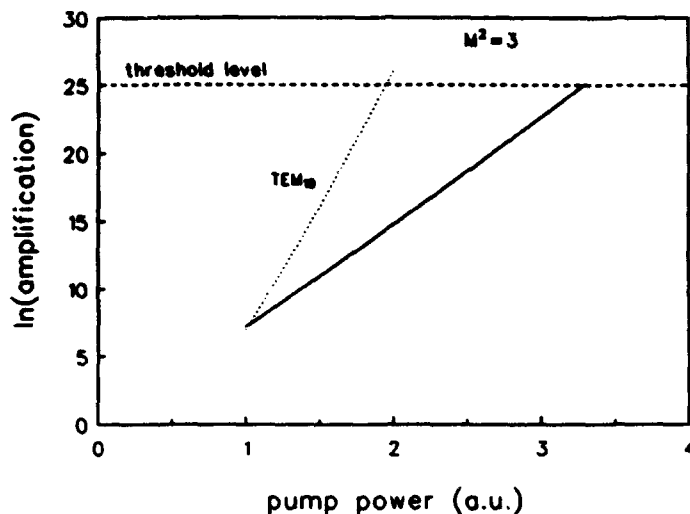


Figure 4.4: Amplification of the Stokes beam versus pump power for a G-L circular symmetric pump beam and a GSM pump beam, both with an  $M^2$  of 3. The solid line indicates the GSM beam and the dotted line indicates the G-L  $TEM_{10}$  beam.

with a high intensity due to the narrow central peak; in contrast with the Gaussian shape where a comparable high beam radius implicates a lower intensity. Furthermore, the shape of the profile does not change while propagating so the high amplification of the center is present during the entire propagation through the Raman cell. In general, the shape of an arbitrary beam changes while propagating thereby reducing the effect of high intensity peaks.

An annular beam profile combines a high beam radius with a low intensity thus a low amplification can be expected meaning a high threshold power. Such a beam profile is the "donut" shape given by

$$\mathcal{E}(x, y, z) = \mathcal{E}_{01}(x, y, z) + i\mathcal{E}_{10}(x, y, z), \quad (4.20)$$

where  $\mathcal{E}_{01}$  and  $\mathcal{E}_{10}$  are the G-H modes of eqn. (4.3). Figure 4.6 shows the beam profiles of the pump and the Stokes beam at threshold power. We found a threshold power that was 40% higher compared to a GSM beam with the same  $M^2$  of 2.0. Since an arbitrary annular beam is in general not shape invariant while propagating through the Raman cell, the amplification of an arbitrary annular beam will be higher because the low intensity ring structure will be lost.

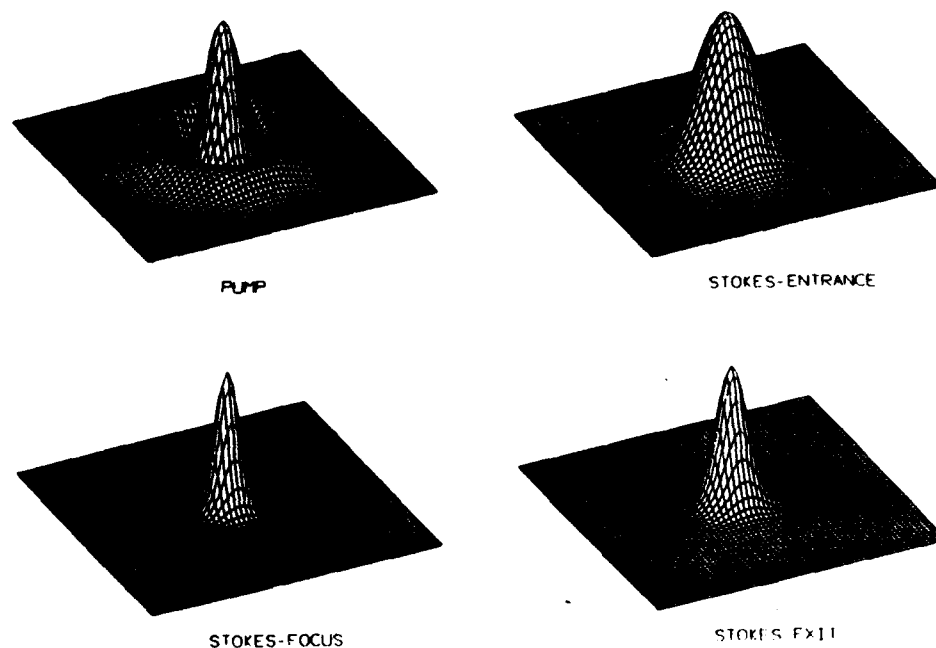


Figure 4.5: Beam profiles, for high pump power, of the circular symmetric G-L  $TEM_{10}$  pump beam and of the Stokes beam at the entrance, middle, and exit of the Raman cell.

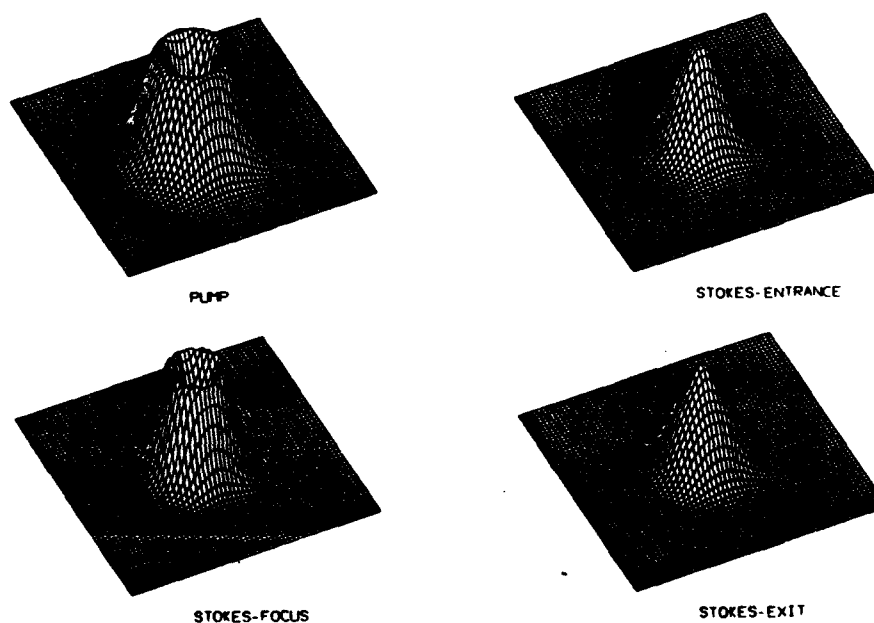


Figure 4.6: Beam profiles at threshold power of the "donut" pump beam and of the Stokes beam at the entrance, middle, and exit of the Raman cell.

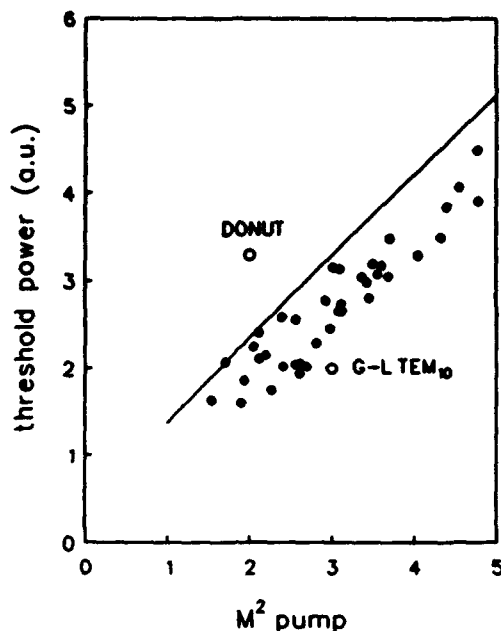


Figure 4.7: Threshold power versus  $M^2$  factor. The closed circles indicate pump beams that are a random superposition of G-H modes; the solid line indicates the GSM pump beams; and the open circles indicate the "donut" shape and the G-L  $TEM_{10}$  mode.

A realistic nondiffraction-limited laser beam does not consist of a single high order mode but of a superposition of several high order modes. Using a random generator, we created several superpositions of G-H modes and used the beam propagation method to obtain the  $M^2$  and the threshold power. To construct the superposition, we used eqn.( 4.3) and

$$\mathcal{E}(x, y, z) = \sum_{0 \leq m \leq 2} \sum_{0 \leq n \leq 2} c_{mn} \mathcal{E}_{mn}(x, y, z), \quad (4.21)$$

where the complex phase factors  $c_{mn}$  are set randomly. Figure 4.7 shows the threshold power versus  $M^2$  for these superpositions and for the GSM beam. It is easily seen that the superpositions have a lower threshold than the GSM beam. This lower threshold is due to the fact that the superpositions have sharp intensity peaks in the beam profile in contrast with the smooth distribution of the GSM beam. Sharp intensity peaks reduce the threshold power due to their higher intensity and due to the gain focusing effect in sharp peaks [33,6]. However, this threshold reduction is at the most 40% of the GSM threshold, therefore the  $M^2$  factor is still a good measure for predicting the experimental threshold. Additionally, figure 4.7 indicates the "donut" shape and the G-L  $TEM_{10}$  mode which shows that these

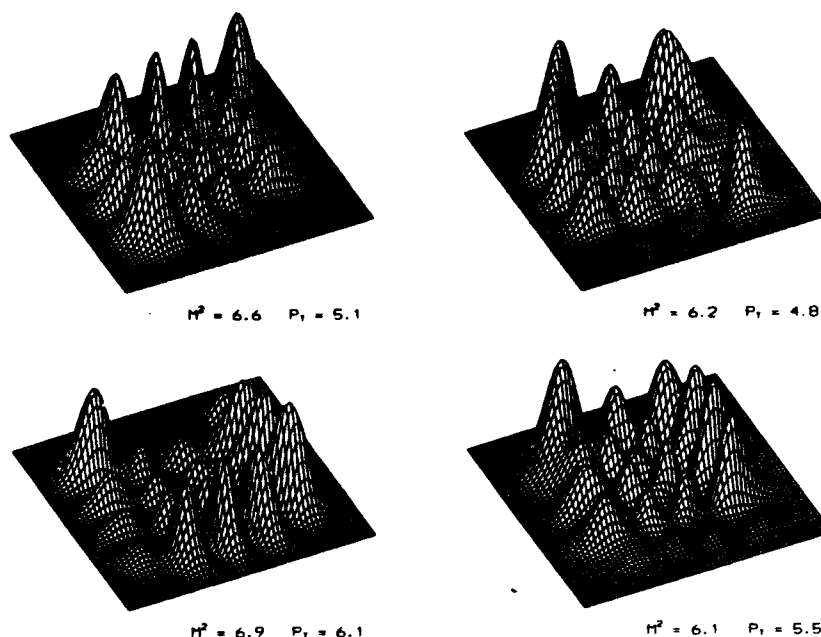


Figure 4.8: Pump beam profiles at the entrance of the Raman cell with corresponding  $M^2$  and threshold power (in arbitrary units).

shapes are extreme cases due to their particular profiles.

The relation between  $M^2$  and the threshold power also holds for profiles with a complicated structure. Figure 4.8 shows four pump profiles of a complicated structure which are a combination of G-H modes with a maximum order of four. In the figure the corresponding  $M^2$  and threshold power (in arbitrary units) are also depicted. The threshold powers are lower than the corresponding thresholds for a GSM beam which are 6.0 and 6.9 (in a.u.) for the  $M^2$  values of 6.0 and 7.0, respectively. As explained in the previous paragraph, this threshold reduction is caused by the sharp intensity peaks. Again this reduction is within 40% of the GSM threshold.

#### 4.3.2 Experimental threshold

Using the experimental set-up described in chapter 3, we measured the Raman threshold for two  $M^2$  values of the pump beam. The  $M^2$  value of the pump beam was varied by changing the diaphragm in the laser. For a diaphragm of 1.5 mm diameter, an  $M^2$  of 1.12 was obtained. An  $M^2$  of 8.7 was obtained for the 6.5 mm diaphragm. Figure 4.9 shows the

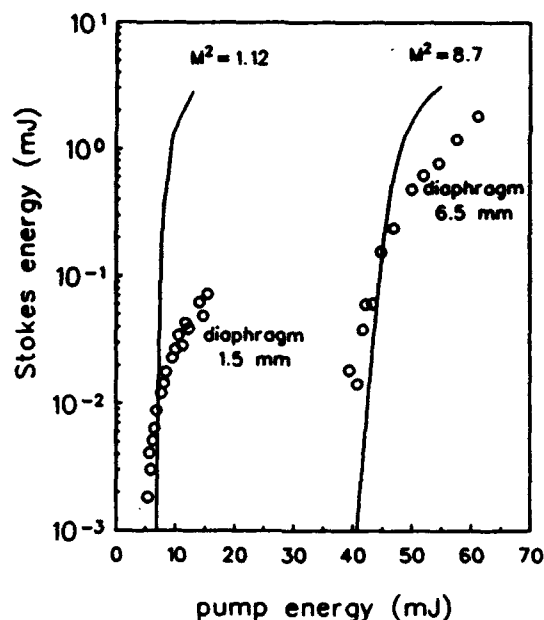


Figure 4.9: Stokes pulse energy versus pump pulse energy near threshold. The circles indicate the experimental data; the solid lines indicate the computer simulation.

threshold measurement for the two diaphragms; as expected, the threshold energy increases with  $M^2$ .

For a correct computer simulation, the reflection coefficient at the windows has to be estimated. Because of the very high gain ( $\approx e^{25}$ ), small reflections of the Stokes beam at the cell windows lower the threshold power since the second amplification more than compensates the reflection loss [22]. The reflection of the backward-scattered-Stokes wavefront at the entrance window is shown in fig. 4.10. A fraction of the beam, typically 0.5%, is reflected at the window, and only a small part of the reflected wavefront is amplified at the focal region. The reflection coefficient is estimated by multiplying the reflection coefficient of the window (0.5%) times the fraction of the wavefront that is amplified. This wavefront fraction is determined with the beam propagation method from the amplification ratio of a divergent and convergent Stokes beam. In this way the following reflection coefficients are determined:  $10^{-5}$  for the pump beam with  $M^2 = 1.12$ , and  $3 \times 10^{-6}$  for  $M^2 = 8.7$ .

With the numerical model, we have simulated the threshold measurements of fig. 4.9. The following input parameters are used: the Raman gain coefficient as obtained from ref. [26], see chapter 3; the reflection coefficient at the cell window; the measured pump power versus

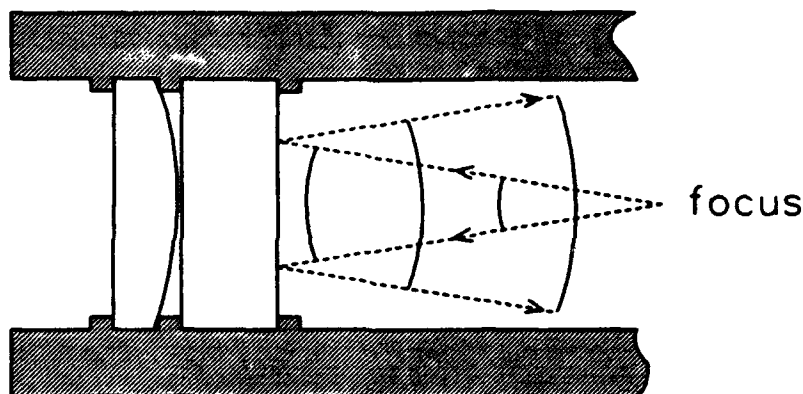


Figure 4.10: Reflection of the Stokes wavefront at the entrance window of the Raman cell.

time; and a GSM pump beam with measured  $M^2$  factor. Figure 4.9 shows the results of the computer simulation as solid lines. It is clear that the threshold energy of the simulations match the experimental results. The efficiency above threshold, however, is not correct. This is due to other effects not included in the model that occur at high pump energy. In chapter 5 these effects, which reduce the conversion efficiency, are studied.

#### 4.4 Conclusions

We have shown that the threshold power of stimulated Raman scattering, for a tightly focused beam, depends mostly on the  $M^2$  factor and to a lesser extent on the exact beam profile. This result has been obtained for high order Gaussian-Hermite and Gaussian-Laguerre beams; for Gaussian-Schell-model beams; and for several superpositions of Gaussian-Hermite modes. For a circular symmetric G-L mode and for a ring shaped G-H superposition, the largest difference in threshold power with the GSM beams occurs. Since this difference is only about 40%, the  $M^2$  factor is a useful parameter for analyzing the experimental threshold. Furthermore, for an arbitrary beam consisting of a superposition of high order modes, we have shown that the difference in threshold power for beams with the same  $M^2$  is often smaller than 40%.

The  $M^2$  factor of a Nd:YAG laser beam has been measured in order to analyze the SRS

threshold for a Raman cell containing high pressure methane. These experimental thresholds correspond with the simulations using a GSM pump beam with the measured  $M^2$  values of 1.12 and 8.7, which confirms the usefulness of  $M^2$  in analyzing threshold measurements.

## 5 OPTIMIZATION OF CONVERSION EFFICIENCY

### 5.1 Introduction

Wavelength conversion at high pump energies is optimized by the use of an astigmatic lens or a pair of cylindrical lenses to focus the pump beam into the Raman cell. Focused beams are used to obtain a high light intensity, which is required for efficient conversion. Approximately, the conversion does not change by varying the focal length of an ordinary lens since the length of the focus times the intensity at the focus is constant [9]. Thus, a shorter focal length results in a shorter Rayleigh range (length of focus) which is compensated by the increased intensity at the focus. However, an astigmatic focus can be used to modify the gain and therefore the conversion [33]. An astigmatic focus gives a tuning facility by varying  $\Delta F$ , i.e. the distance between the two foci.

In the experimental study, a Nd:YAG laser was focused into a Raman cell containing 88 bar of methane. The conversion of the pump beam to other wavelengths was studied as a function of pump energy for an ordinary and for an astigmatic focus. We monitored the energy at the following generated wavelengths: the first Stokes at 1.5  $\mu\text{m}$ , the second Stokes at 2.8  $\mu\text{m}$ , the anti-Stokes at 0.8  $\mu\text{m}$ , and the Brillouin scattering at 1.06  $\mu\text{m}$ . A dichroic mirror, transparent for the pump and highly reflective for the first Stokes, was placed at the entrance of the cell to enhance the first-Stokes generation.

Numerical simulations were performed and compared with the experimental results. All the input parameters were obtained from the literature and none of the parameters were fitted to match the simulations to the experiments. Ground-state depletion, i.e. reduction of the density of atoms or molecules in the ground state, was investigated numerically. This saturation effect occurs when the relaxation time of the final Raman level is long compared to the pulse width of the laser, as is the case in our experiments. Under these conditions, the number of generated Stokes photons is limited by the number of molecules in the volume where the conversion takes place.

## 5.2 Theory

### 5.2.1 Raman amplification

To reduce the complexity, the powers of the Stokes and the pump beam are used instead of the full beam profile. The transverse intensity is accounted for in the model through the area of the pump beam as a function of  $z$ . The Raman propagation is then described by coupled nonlinear equations for the pump power and for the forward- and backward-traveling Stokes powers [1,37]:

$$\frac{n}{c} \partial_t F + \partial_z F = A(z)(F + \delta)P, \quad (5.1)$$

$$\frac{n}{c} \partial_t B - \partial_z B = A(z)(B + \delta)P, \quad (5.2)$$

$$\frac{n}{c} \partial_t P + \partial_z P = -\frac{k_p}{k_s} A(z)(F + B + 2\delta)P, \quad (5.3)$$

where  $P(z, t)$ ,  $F(z, t)$ , and  $B(z, t)$  are the pump power, the forward scattered Stokes power, and the backward scattered Stokes power, respectively;  $c/n$  is the speed of light in the medium; and  $\delta$  is the spontaneous Raman noise power. The gain  $A(z)$  is given by

$$A(z) = \frac{g}{A(z)} \eta, \quad (5.4)$$

where  $g$  is the Raman gain coefficient,  $A(z)$  is the cross-sectional area of the pump beam as a function of  $z$ , and  $\eta$  is a factor describing the gain focusing effect. A value of 1.6 for  $\eta$  was obtained with the beam propagation method described in chapter 2. The cross-sectional area of the pump beam is

$$A(z) = \pi w_x(z)w_y(z), \quad (5.5)$$

where  $2w_x$  and  $2w_y$  are the beam diameters in the  $x$ - and  $y$ -direction, referring to the  $1/e^2$  intensity points.

Second-Stokes generation by a cascade process, where the first Stokes is shifted by SRS, can be included by using similar equations with the forward first-Stokes power instead of the pump power:

$$\frac{n}{c} \partial_t F_2 + \partial_z F_2 = A_2(z)(F_2 + \delta)F, \quad (5.6)$$

$$\frac{n}{c} \partial_t B_2 - \partial_z B_2 = A_2(z)(B_2 + \delta)F, \quad (5.7)$$

where  $F_2(z, t)$  and  $B_2(z, t)$  are the forward scattered second-Stokes power and the backward scattered second-Stokes power, respectively. The gain  $A_2(z)$  is given by (5.4) using the Raman gain coefficient  $g$  at the first-Stokes wavelength. The propagation of the forward first-Stokes beam has to be modified with depletion due to second-Stokes generation:

$$\begin{aligned} \frac{n}{c} \partial_t F + \partial_z F &= A(z)(F + \delta)P \\ &\quad - \frac{k_z}{k_{s2}} A_2(z)(F_2 + B_2 + 2\delta)F. \end{aligned} \quad (5.8)$$

Backward first Stokes can be ignored as a pump source since the dichroic mirror at the entrance window causes the forward first Stokes to be much more intense. This assumption was also checked numerically; adding a similar set of equations with  $B$  as pump had a negligible influence on second-Stokes generation.

Second-Stokes generation by four-wave mixing is not taken into account since the wave-vector mismatch is large for high pressure methane. Using the data presented in ref. [38], we obtain a wave-vector mismatch  $\Delta k$  of  $14.6 \text{ cm}^{-1}$  for  $\text{CH}_4$  at 88 bar. The phase-match angle given by  $\sqrt{k_p \Delta k / k_{s2} k_s}$  is 30 mrad. The divergence of the pump beam is 25 mrad given the beam radius of 0.25 cm at the entrance window and a focal length of 10 cm. Since the divergence of the pump beam is smaller than the phase-match angle, four-wave mixing is suppressed. Furthermore, the pump beam is far from diffraction limited, which also reduces four-wave mixing.

An experimental complication are the small but significant reflections at the windows of the Raman cell. Because of the very high gain ( $e^{25}$  at threshold), a small reflection can still decrease the threshold energy [22]. Here the term threshold means the pump power corresponding to 1 percent conversion efficiency [27]. Therefore, the input parameters include the reflection coefficient of the windows.

### 5.2.2 Ground-state depletion

Stimulated Raman scattering induces a transition of the methane molecule from the ground state to an excited state. If the lifetime of the vibrationally excited state is much longer than the pulse duration, the number of molecules in the ground state will diminish [19]. Since each excited molecule corresponds to one scattered pump photon producing a single

Stokes photon, the following conservation law applies:

$$\partial_t N + \frac{1}{\hbar\omega_s} \partial_z (I_F - I_B) = 0, \quad (5.9)$$

where  $N$  is the number density of methane molecules in the ground state,  $I_F$  is the forward Stokes intensity,  $I_B$  is the backward Stokes intensity, and  $\hbar\omega_s$  is the energy of the Stokes photon.

Ground-state depletion will reduce the amplification, which is proportional to  $N$  and expressed by

$$A(z, t) = \frac{g\eta}{A(z)} \cdot \frac{N(z, t)}{N_0}, \quad (5.10)$$

where  $N_0$  is the initial undepleted density. Combining (5.9) and (5.10), we obtain for  $A$ :

$$\partial_t A = \frac{g\eta}{N_0 A^2 \hbar\omega_s} (\partial_z B - \partial_z F) \quad (5.11)$$

This equation is implemented in the numerical method to study ground-state depletion.

### 5.3 Experiment

Details of the experimental setup are described in chapter 3. A Q-switched Nd:YAG laser was used to generate the pump beam. The laser provided  $1.06 \mu\text{m}$  pulses up to 350 mJ in energy with a FWHM pulse width of 7 ns. The beam quality, i.e. the  $M^2$  factor, was measured using a standard knife-edge technique giving an  $M^2$  of 8.7. Details of the  $M^2$  measurement are described in chapter 3. The energy of the laser beam was adjusted by an attenuator before the beam entered the Raman cell.

The 20 cm long Raman cell contained methane with a pressure of 88 bar. At the entrance of the Raman cell a dichroic mirror was placed to reflect the backward scattered Stokes into the Raman cell in order to obtain all Stokes radiation in the forward direction.

An estimation of the spontaneous Raman noise is made using the spontaneous intensity  $\Gamma\hbar\omega_s/4A$  as derived in [30]. A noise power  $\delta$  of  $10^{-9}$  W is obtained in this way. Correcting for the higher divergence of a nondiffraction-limited pump beam, we obtain a noise power  $\delta$  of  $M^4 \times 10^{-9}$  W, i.e.  $10^{-7}$  W. These literature values were used in the numerical model described above.

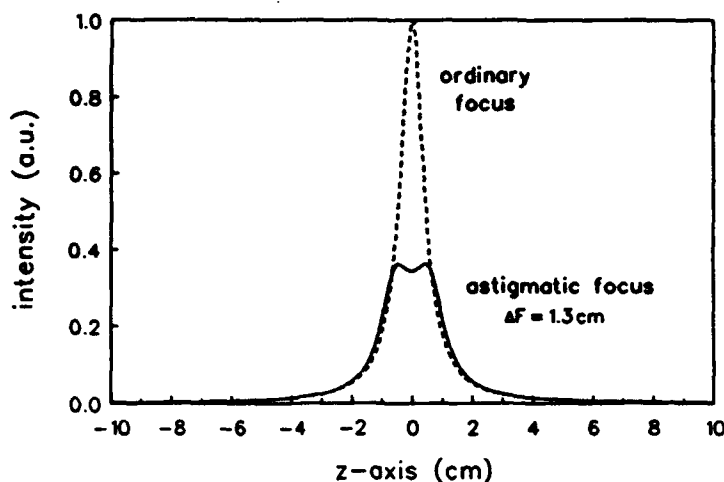


Figure 5.1: Intensity of the pump on the optical axis for an ordinary focus (dashed line) and for an astigmatic focus (solid line).

The pump beam was focused into the Raman cell by an ordinary spherical lens of 10 cm focal length or by a pair of cylindrical lenses of 10 cm focal length placed 1.3 cm apart. For a nondiffraction-limited beam, the Rayleigh range is given by  $z_R = kw_0^2/(2M^2)$ , where  $w_0$  is the beam radius at the focus. The divergence of the focused beam is 0.025 rad given the beam radius of 0.25 cm at the entrance window and a focal length of 10 cm. We obtain a Rayleigh range of 0.47 cm using the expression for the Rayleigh range and the following expression for the divergence:  $\phi = w_0/z_R$ . With this Rayleigh range, we can calculate the intensity on the optical axis given by

$$I_{\text{axis}}(z) = I_0 \frac{w_0^2}{w(z + \Delta F/2)w(z - \Delta F/2)} \quad (5.12)$$

using the following expression for the beam radius:

$$w^2(z) = w_0^2(1 + z^2/z_R^2). \quad (5.13)$$

Figure 5.1 shows the intensity on the optical axis for the ordinary and the astigmatic focus. It is clear that the intensity is significantly reduced for the astigmatic focus.

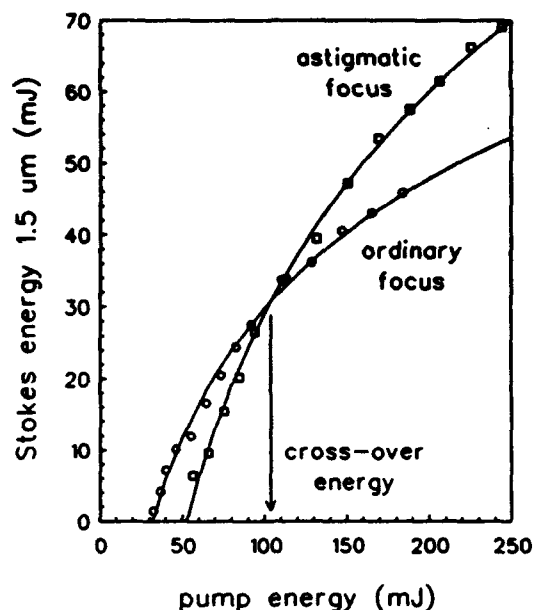


Figure 5.2: Measured Stokes energy versus pump energy for an ordinary focus and an astigmatic focus. The lines are a guide to the eye only.

#### 5.4 Results and Discussion

Using the experimental setup described above, we measured the Stokes energy as a function of pump energy for a spherical lens and for an astigmatic lens. Figure 5.2 shows the experimental results. The maximum photon conversion efficiency in the cell is 55% at 170 mJ giving 54 mJ of Stokes energy. Here we have taken into account reflection losses of 5% at the entrance and 12% at the exit. The high reflection losses are caused by the dichroic mirror at the entrance and by the  $\text{CaF}_2$  window and collimating lens at the exit. Uncoated  $\text{CaF}_2$  was used in order to measure the second Stokes at  $2.8 \mu\text{m}$  which is strongly absorbed by glass. At high pump energy an astigmatic focus gives a higher Stokes energy compared to an ordinary focus. The cross-over energy, i.e. the pump energy where the ordinary and the astigmatic focus give the same Stokes energy, is 104 mJ as obtained from figure 5.2.

Radiation from competing, nonlinear processes have also been measured. Figure 5.3 shows the stimulated Brillouin scattering (SBS) energy. It is clear that the SBS is negligible since the maximum energy is only 2.5 mJ. Anti-Stokes radiation at  $0.8 \mu\text{m}$  is shown in figure 5.4 and is clearly negligible. Second Stokes at  $2.8 \mu\text{m}$  is not negligible at high energy

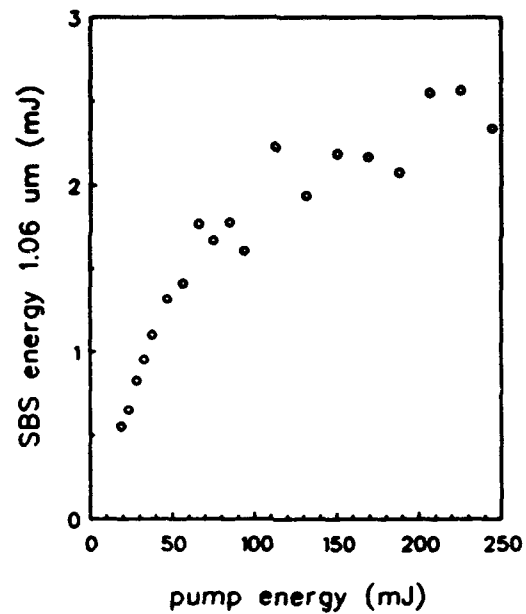


Figure 5.3: Stimulated-Brillouin-scattering energy versus pump energy for an astigmatic focus.

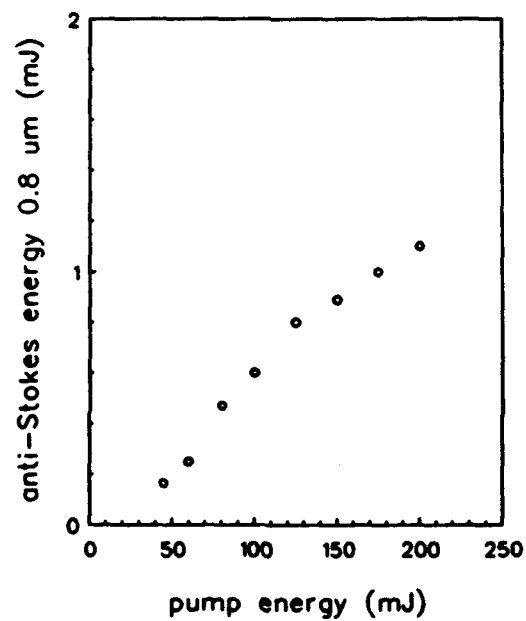


Figure 5.4: Anti-Stokes energy versus pump energy for an astigmatic focus.

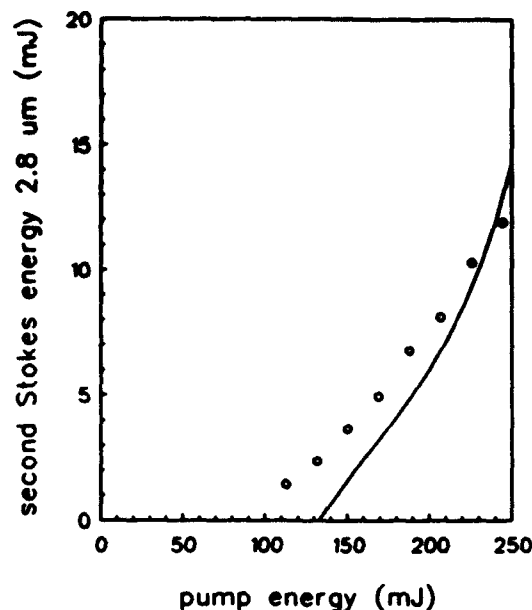


Figure 5.5: Second-Stokes energy versus pump energy for an astigmatic focus. The solid line indicates the simulation.

as figure 5.5 shows. It has to be noted that we could only measure the second Stokes in the forward direction since the entrance window absorbed the  $2.8 \mu\text{m}$ . At 250 mJ pump energy, the second Stokes is 12 mJ, which implies that it is one third in photon number of the first Stokes of 70 mJ. Therefore, second-Stokes generation appears to be an important limiting factor for first-Stokes generation at high pump energy.

Numerical calculations were performed to study the limiting processes for  $1.5 \mu\text{m}$  generation. Because of the very high gain ( $> e^{25}$ ), small reflections at the cell windows lower the threshold power since the second amplification more than compensates the reflection loss [22]. The effective reflections are small since the beam reflected at a window is not focused, so only the fraction of the beam that is reflected into the focus has to be taken into account. Using the procedure described in [39], we obtained the following reflection coefficients: 1.0 (dichroic mirror) and  $5 \times 10^{-5}$  at  $1.54 \mu\text{m}$  for the entrance and exit window, respectively; and  $5 \times 10^{-5}$  at  $2.8 \mu\text{m}$  for both windows.

Figure 5.6 shows the Stokes energy as a function of pump energy for both lenses using the numerical method presented earlier. The cross-over energy according to the simulation is 111 mJ, which is in good agreement with the experimental value of 104 mJ. Second-Stokes

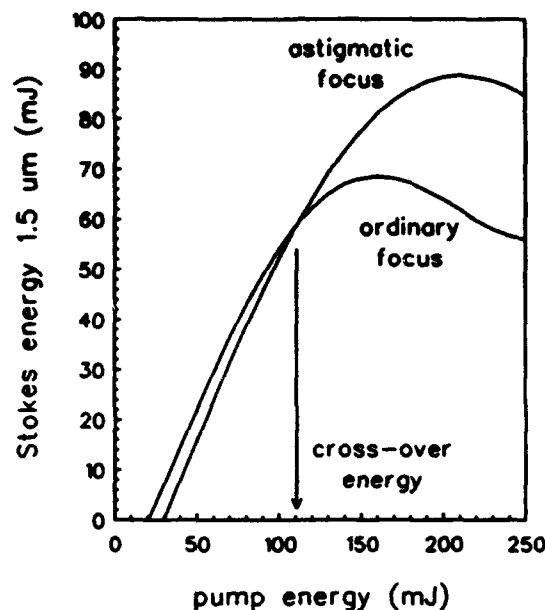


Figure 5.6: Simulated Stokes energy versus pump energy for an ordinary focus and an astigmatic focus.

simulation is depicted in figures 5.5 and 5.7, showing at least a qualitative agreement with the experiments. The effect of the astigmatic focus is a reduction of the gain [33], which also reduces the gain for second-Stokes generation resulting in a higher conversion above the cross-over energy.

The difference between experiment and simulation can be attributed to the simplification of ignoring the transverse intensity of the beams. A consequence of the transverse beam profile is that the pump energy at the beam edge is not so easily converted as the energy at the center. This edge effect is not taken into account by the simulation, which results in a higher Stokes energy. A more extensive numerical method using the transverse intensities should give a better correspondence of simulation and experiment. We hope to extend our model in the future with the transverse intensities.

Ground-state depletion is another process that can limit the conversion efficiency. Since the amplification takes place predominantly in the focal region, a natural approach is to calculate the number of molecules in this region, which should correspond to the maximum number of generated Stokes photons. Using the Rayleigh range  $z_R$  and the spot size  $w_0^2$ , which were derived above, we obtain a volume for the focal region of  $4 \times 10^{-4} \text{ cm}^3$  using

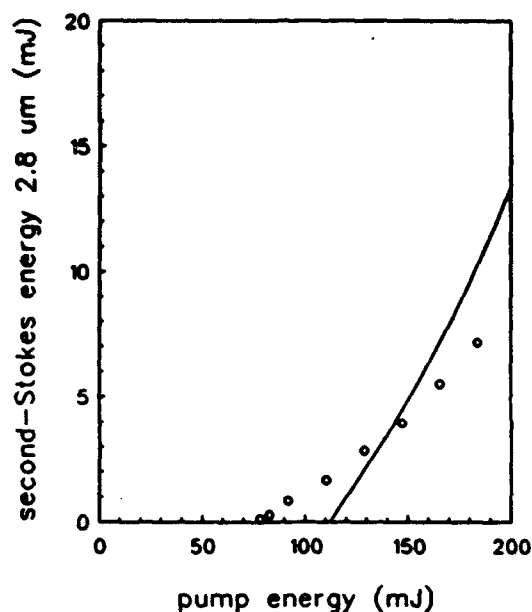


Figure 5.7: Second-Stokes energy versus pump energy for an ordinary focus. The solid line indicates the simulation.

$2z_R \times \pi w_0^2$ . This volume corresponds to  $10^{18}$  molecules giving a maximum Stokes energy of 130 mJ using the Stokes photon energy of  $1.3 \times 10^{-19}$  J. Since the generated Stokes energy is of the same order of magnitude, we expected a considerable influence of ground-state depletion (GSD). However, numerical calculations show a negligible influence of GSD when the simulations with and without GSD are compared. For an ordinary focus at a pump energy of 250 mJ, a Stokes energy of 133.2 mJ was obtained without GSD and 133.1 mJ was obtained with GSD (second-Stokes generation was not used in this simulation). Figure 5.8 shows  $(N_0 - N(z))A(z)$  versus  $z$ , which is the quantity that indicates where the molecules are excited; the area under the curve is the number of excited molecules, i.e.  $10^{18}$  corresponding with the 133.1 mJ Stokes energy. It is clear that the majority of excited molecules is outside the focal region, which results in a much lower GSD effect.

Experiments with several methane pressures were performed to check whether the GSD is negligible. At lower methane pressures the number of molecules that are available for SRS decreases which would result in a lower Stokes energy at high pump energies. Figure 5.9 shows the Stokes energy versus the pump energy for methane pressures of 50, 70, and 90 bar. It is clear that there is no significant reduction for low pressures at high pump energies,

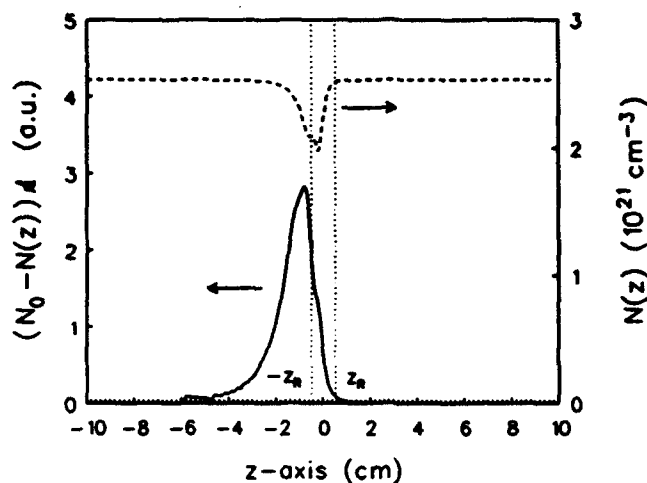


Figure 5.8: Ground-state depletion given by  $(N_0 - N(z))A$  versus  $z$  (solid line); and number density of molecules in the ground state (dashed line).

therefore GSD does not occur. The lower Stokes energy at low pump power is due to the lower gain as a consequence of the lower methane pressure.

## 5.5 Conclusions

It has been shown that the conversion efficiency at high pump energy of a Raman cell can be improved by an astigmatic focus. Our experiments show that second-Stokes generation by a cascade process is the principal limiting factor for high efficiency first-Stokes conversion. Brillouin scattering and anti-Stokes generation were negligible. Measurements at several methane pressures indicate that the first-Stokes generation is not limited by ground-state depletion. An astigmatic focus reduces the gain, which leads to a lower efficiency at low pump power but a higher efficiency at high pump power due to the lower gain of the second-Stokes generation.

Numerical simulations were performed and compared with the experimental results. The experiments and simulations correspond reasonably well taken into account that all input parameters were obtained from the literature and none of the parameters were fitted to match the simulation to the experiment. Good agreement was obtained for the cross-over energy, i.e. the pump energy where the ordinary and the astigmatic focus give the same

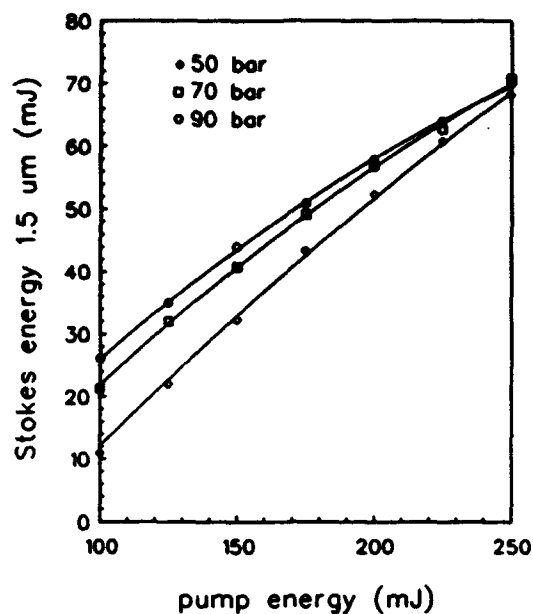


Figure 5.9: Measured Stokes energy versus pump energy for various methane pressures. The lines are a guide to the eye only.

Stokes energy, namely 104 mJ for the experiment and 111 mJ for the simulation. Ground-state depletion was also investigated numerically. It has been shown that the majority of the excited molecules is outside the focal region, which causes the effect of ground-state depletion to be negligible.

## 6

## CONCLUSIONS

In this report wavelength conversion by stimulated Raman scattering (SRS) has been investigated using experimental and numerical methods. The experimental setup consisted of a Nd:YAG laser and a high pressure methane Raman cell for the conversion of the 1.06  $\mu\text{m}$  radiation to the eye-safe 1.54  $\mu\text{m}$  wavelength. Emphasis is on the identification and modeling of the relevant physical processes involved in the wavelength conversion. Optimization of the setup towards practical application is described in previous reports [3,4]. Both the low and the high pump power regime have been investigated.

A three-dimensional finite difference method has been presented for the propagation of beams focused by an astigmatic lens. This FD method is stable and unitary, which means that the power of the beams is conserved. The FD method is used for the modeling of a Raman amplifier. The results of the FD method have been cross-checked with analytical models and with a numerical model that describes gain focusing. It has been shown that the FD method gives reliable results both for low and for high pump power.

Numerical simulations have shown that the threshold power of stimulated Raman scattering, for a tightly focused beam, depends mostly on the  $M^2$  factor and to a lesser extent on the exact beam profile. This result has been obtained for high order Gaussian-Hermite and Gaussian-Laguerre beams; for Gaussian-Schell-model beams; and for several superpositions of Gaussian-Hermite modes. For a circular symmetric G-L mode and for a ring shaped G-H superposition, the largest difference in threshold power with the GSM beams occurs. Since this difference is only about 40%, the  $M^2$  factor is a useful parameter for analyzing the experimental threshold. Furthermore, for an arbitrary beam consisting of a superposition of high order modes, we have shown that the difference in threshold power for beams with the same  $M^2$  is often smaller than 40%. The  $M^2$  factor of a Nd:YAG laser has been measured in order to analyze the SRS threshold for a Raman cell containing high pressure methane. These experimental thresholds correspond with the simulations using a GSM pump beam with the measured  $M^2$  values of 1.12 and 8.7, which confirms the usefulness of  $M^2$  in analyzing threshold measurements.

It has been shown that the conversion efficiency at high pump energy of a Raman cell can be improved by an astigmatic focus. Our experiments show that second-Stokes generation by a cascade process is the principal limiting factor for high efficiency first-Stokes conversion. An astigmatic focus reduces the gain, which leads to a lower efficiency at low pump power but a

higher efficiency at high pump power due to the lower gain of the second-Stokes generation. Numerical simulations were performed and compared with the experimental results. The experiments and simulations correspond reasonably well taken into account that all input parameters were obtained from the literature and none of the parameters were fitted to match the simulation to the experiment. Good agreement was obtained for the cross-over energy, i.e. the pump energy where the ordinary and the astigmatic focus give the same Stokes energy, namely 104 mJ for the experiment and 111 mJ for the simulation. Ground-state depletion was also investigated numerically. It has been shown that the majority of the excited molecules is outside the focal region, which causes the effect of ground-state depletion to be negligible. Measurements at several methane pressures confirm that the first-Stokes generation is not limited by ground-state depletion.

We believe that our numerical model will be a useful tool for analyzing and predicting the performance of various conversion setups with variation in wavelength, pulse width, pulse energy,  $M^2$  value, and Raman medium.

## REFERENCES

- [1] J.C. White, "Stimulated Raman scattering," in *Tunable Lasers*, ch. 4, Springer-Verlag, 1987.
- [2] R.W. Nichols and W.K. Ng, "Raman shifted Nd:YAG class 1 eye-safe laser development," *SPIE Scientific and Engineering applications of commercial laser devices*, vol. 610, pp. 92-98, 1986.
- [3] F.J.M. van Putten, "Generation of high power 1.54  $\mu\text{m}$  radiation by stimulated Raman scattering in methane," Tech. Rep., TNO Physics and Electronics Laboratory, 1990. (in Dutch).
- [4] F.J.M. van Putten, J.C. van den Heuvel, and R.L.J. Lerou, "First and second order stokes generation by srs in methane: influence of rep-rate, beam quality and astigmatism," Tech. Rep., TNO Physics and Electronics Laboratory, 1990.
- [5] H. Kogelnik, "On the propagation of gaussian beams of light through lenslike media including those with a loss or gain variation," *Appl. Opt.*, vol. 4, pp. 1562-1569, 1965.
- [6] D. Cotter, D.C. Hanna, and R. Wyatt, "Infrared stimulated Raman generation: effect of gain focussing on threshold and tuning behaviour," *Appl. Phys.*, vol. 8, pp. 333-340, 1975.
- [7] B.N. Perry, P. Rabinowitz, and M. Newstein, "Wave propagation in media with focused gain," *Phys. Rev. A*, vol. 27, pp. 1989-2002, 1983.
- [8] T.F. Johnston Jr., " $M^2$  concept characterizes beam quality," *Laser Focus World*, pp. 173-183, May 1990.
- [9] M.L. Bhaumik, "Physics of Raman lasers," *Am. J. Phys.*, vol. 35, pp. 330-335, 1967.
- [10] F.J.M. van Putten, "Working paper of: generation of high power 1.54  $\mu\text{m}$  radiation by stimulated Raman scattering in methane," 1990.
- [11] R.T. Kung, "Multiple pass stimulated Raman conversion with pump depletion," *IEEE J. Quantum Electron.*, vol. 17, pp. 509-513, 1981.
- [12] G.D. Boyd, Jr. W.D. Johnston, and I.P. Kaminow, "Optimization of the stimulated Raman scattering threshold," *IEEE J. Quantum Electron.*, vol. 5, pp. 203-206, 1969.
- [13] K.J. Druhl, S. Shakir, and M. Yousaf, "Approximate theory of Stokes amplification and conversion valid at large gain," *Opt. Lett.*, vol. 11, pp. 446-448, 1986.

- [14] A. Yariv, *Quantum Electronics*, ch. 6. New York: Wiley, 2nd ed., 1975.
- [15] W.H. Press, B.P. Flannery, S.A. Teukolsky, and W.T. Vetterling, *Numerical Recipes*, ch. 17. Cambridge University Press, 1986.
- [16] W.F. Ames, *Numerical Methods for Partial Differential Equations*. Academic Press, New York, 1977.
- [17] F.R. Gantmacher, *The Theory of Matrices*, p. 279. Vol. 1, Chelsea Publishing Company, New York, 1977.
- [18] J. Eggleston and R.L. Byer, "Steady-state stimulated Raman scattering by a multimode laser," *IEEE J. Quantum Electron.*, vol. 16, pp. 850-853, 1980.
- [19] E. Margalith and G.W. Sutton, "A theoretical analysis of stimulated Raman conversion," *J. Appl. Phys.*, vol. 59, pp. 327-331, 1985.
- [20] G.R. Hadley, "Transparent boundary condition for the beam propagation method," *IEEE J. Quantum Electron.*, vol. 28, pp. 363-370, 1992.
- [21] Y. Chung and N. Dagli, "An assessment of finite difference beam propagation method," *IEEE J. Quantum Electron.*, vol. 26, pp. 1335-1339, 1990.
- [22] G. Haidacher and M. Maier, "Explanation of anomalies in the stimulated Raman scattering in H<sub>2</sub> gas," in *VIII Intern. Quant. Electron. Conf.*, (San Francisco), pp. 786-787, 1974.
- [23] O.N. Krokhin, "Generation of high-temperature vapors and plasmas by laser radiation," in *Laser Handbook*, (F.T. Arecchi and E.O. Schulz-Dubois, eds.), North-Holland Publishing Company, 1972.
- [24] P. Chylek, M.A. Jarzembski, V. Srivastava, and R.G. Pinnick, "Pressure dependence of the laser-induced breakdown thresholds of gases and droplets," *Appl. Opt.*, vol. 29, pp. 2303-2306, 1990.
- [25] C.G. Parazzoli, W.W. Buchman, and R.D. Stultz, "Numerical and experimental investigation of a stimulated Raman half resonator," *IEEE J. Quantum Electron.*, vol. 24, pp. 872-880, 1988.
- [26] J.J. Ottusch and D.A. Rockwell, "Measurement of Raman gain coefficients of hydrogen, deuterium, and methane," *IEEE J. Quantum Electron.*, vol. 24, pp. 2076-2080, 1988.
- [27] D.C. Hanna, D.J. Pointer, and D.J. Pratt, "Stimulated Raman scattering of picosecond light pulses in hydrogen, deuterium, and methane," *IEEE J. Quantum Electron.*, vol. 22, pp. 332-336, 1986.

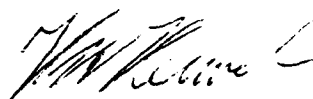
- [28] H.W. Schrotter and H.W. Klockner, "Raman scattering cross sections in gases and liquids," in *Raman Spectroscopy of Gases and Liquids*, ch. 4, Springer-Verlag, 1979.
- [29] R.C. Weast, ed., *Handbook of Chemistry and Physics*. The Chemical Rubber Company, 1970. 51<sup>st</sup> edition.
- [30] A.T. Georges and S.N. Dixit, "Dependence of broadband Raman amplification in dispersive media on the pump-stokes input correlation," *J. Opt. Soc. Am. B*, vol. 8, pp. 780-785, 1991.
- [31] A.E. Siegman, M.W. Sasnett, and T.F. Johnston Jr., "Choice of clip levels for beam width measurements using knife-edge techniques," *IEEE J. Quantum Electron.*, vol. 27, pp. 1098-1104, 1991.
- [32] F. Gori and M. Santarisiero, "The change of width for a partially coherent beam on paraxial propagation," *Opt. Commun.*, vol. 82, pp. 197-203, 1991.
- [33] J.C. van den Heuvel, "Numerical modeling of stimulated Raman scattering in an astigmatic focus," *IEEE J. Quantum Electron.*, vol. 28, pp. 378-385, 1992.
- [34] H. Kogelnik and T. Li, "Laser beams and resonators," *Appl. Opt.*, vol. 5, pp. 1550-1567, 1966.
- [35] R. Gase, "The multimode laser radiation as a gaussian schell model beam," *J. Mod. Opt.*, vol. 38, pp. 1107-1115, 1991.
- [36] A.E. Siegman, "Defining the effective radius of curvature for a nonideal optical beam," *IEEE J. Quantum Electron.*, vol. 27, pp. 1146-1148, 1991.
- [37] G.I. Kachen and W.H. Lowdermilk, "Relaxation oscillations in stimulated Raman scattering," *Phys. Rev. A*, vol. 16, pp. 1657-1664, 1977.
- [38] Z. Chu, U.N. Singh, and T.D. Wilkerson, "Multiple Stokes wavelength generation in H<sub>2</sub>, D<sub>2</sub>, and CH<sub>4</sub> for lidar aerosol measurements," *Appl. Opt.*, vol. 30, pp. 4350-4357, 1991.
- [39] J.C. van den Heuvel, F.J.M. van Putten, and R.J.L. Lerou, "The stimulated Raman scattering threshold for a nondiffraction-limited pump beam," *IEEE J. Quantum Electron.*, vol. 28, pp. 1930-1936, 1992.

---



R.J.L. Lerou  
(Groupleader)

---



J.C. van den Heuvel  
(Author)

## RUNNING THE PROGRAM

At the time of this writing, the program resides in the directory /mnt/heun4/bin on the file system of the CONVEX C230. Copy the files rambo and small.inp to your directory, so you can run the program by typing

```
rambo small
```

Here, rambo is the program name (Raman Amplification Method with Beam Options) and small stands for the input file small.inp. During the execution, the program writes the following information to your screen:

```
rambo (Raman Amplification Method with Beam Options) version 1.0; 93.4.19
```

```
z_axis start value is :      0
z_axis stop value is :      20
place of x-focus      10 - Rayleigh length x-focus      1.64
grid reduction at x-focus 0.162
place of y-focus      10 - Rayleigh length y-focus      1.64
grid reduction at y-focus 0.162
```

```
***** beam propagation method *****
```

```
pump power : 1.534e6
```

z	step	widthX	widthY	dz/kdx <sup>2</sup>	gA=area	gA/bA	tot_flux
0.000	0.2000	3.12e-3	3.12e-3	0.4096	7.85e-3	7.958	30.68
2.000	0.2000	2.52e-3	2.52e-3	0.6307	5.10e-3	7.957	30.68
4.000	0.1000	1.92e-3	1.92e-3	0.5435	2.96e-3	7.954	30.68
6.000	0.05000	1.33e-3	1.33e-3	0.5624	1.43e-3	7.949	30.68
8.000	0.02500	7.98e-4	7.98e-4	0.7848	5.13e-4	7.944	30.68
10.00	0.01250	5.07e-4	5.07e-4	0.9737	2.06e-4	7.966	30.68
12.00	0.02500	7.98e-4	7.98e-4	0.7848	5.10e-4	7.994	30.68
14.00	0.05000	1.33e-3	1.33e-3	0.5624	1.42e-3	7.991	30.68
16.00	0.1000	1.92e-3	1.92e-3	0.5435	2.95e-3	7.987	30.68
18.00	0.2000	2.52e-3	2.52e-3	0.6307	5.08e-3	7.984	30.68
20.00	0.2000	3.12e-3	3.12e-3	0.4096	7.83e-3	7.983	30.68

```
***** time profile and plane-wave approximation *****
```

```
pump pulse duration : 1.50e-8
```

pump pulse energy : 8.00e-3  
pump maximum power : 1.534e6  
gain focusing factor : 1.273

(minimum) number of iterations time profile & plane wave: 4893

#iterations	time	energy_in_cell
0	0.000	0.000
899	3.00e-9	7.21e-4
1797	5.99e-9	8.58e-4
2695	8.99e-9	2.05e-4
3593	1.20e-8	1.46e-5
4492	1.50e-8	3.48e-7
4893	1.63e-8	0.000

With this output, it is possible to check whether the simulation gives valid results. The beam propagation method uses an adaptable  $\Delta z$  listed under step, which is reduced at the focus to keep  $\Delta z/k(\Delta x)^2$  below a certain constant (here 1.0). widthX and widthY are the  $\Delta x$  and  $\Delta y$  of the two-dimensional grid; the area of the grid is listed under gA=area. A useful check is whether the beams are well mapped on the grid, which can be monitored by the column gA/bA showing the ratio of the grid area and the pump beam area. For a good mapping, this ratio should be around 10. Another test is the photon flux given in arbitrary units by tot\_flux, which should be constant.

In the time profile and plane-wave approximation, general information about the pump pulse is given. The energy in the cell is monitored and the iteration stops at the point where this energy is negligible. Units are not listed in the output, but this is no real draw-back since all dimensions have fixed units: length scales are in centimeters, time is in seconds, power is in Watt, and energy is in Joule.

As was already mentioned, this output was produced for an input file small.inp. Here follows the contents of small.inp:

Input file for the Stimulated Raman Scattering program: rambo.

This is an example input file showing a minimal number of entries.  
The values are only listed as an example and do not reflect a realistic experiment.  
The units between [] are comments only, just as the characters after /\*.

**GENERAL INPUT PARAMETERS**

```
end_z_axis = 20.0 [cm] /* length Raman cell */
pump_place_x_focus = 10.0 [cm] /* position of focus (in x-z plane) */
pump_x_width/2 = 0.05 [cm] /* beam width (half diameter at 1/e2 points) */
pump_wavenumber = 5e4 [1/cm] /* wavenumber in medium (not free space) */
raman_gain_stokes = 5e-10 [cm/W] /* Raman gain coefficient */
```

**BEAM PROPAGATION METHOD** : uses 2-dim grid for beam profile

```
beam_propagation = on /* on or off; skip this method when off */
```

```
/* these two entries are not used if time_plane_wave is on */
pump_power = 2.50e6 [W] /* more than one value is allowed */
stokes_power = 1.00e-19 [W] /* more than one value is allowed, but use the
    same number as with pump_power */
```

**TIME-PROFILE AND PLANE-WAVE APPROXIMATION**

```
time_plane_wave = on /* on or off; time profile and plane wave approx. */
```

```
pulse_width = 5e-9 [s] /* Used when pump_profile_file is auto; FWHM */
pump_energy = 8.0e-3 [J] /* scales the pump power to this energy;
    more than one value is allowed */
```

**OUTPUT SPECIFICATIONS**

```
out_silent = off /* off means output to stdout, on means silent */
```

It is clear that a complete simulation, with beam propagation and time dependence simulation, can be done with a limited number of input parameters. However, the total number of parameters used for this simulation is much higher, but these other parameters are given a default value. In the output file `small.otp`, the default values are listed. A list of all parameters are given in appendix B.

Now we have arrived at the point where we can examine the results of the simulation. The output of the program is written to file `small.otp`. Since this file is rather long, parts of the file are replaced by two lines with dots:

```
... [like this]
```

```
...
```

Here follows the contents of small.otp

# OUTPUT FILE

rambo (Raman Amplification Method with Beam Options) version 1.0; 93.4.19

information from the input file :

(standard units : length [cm], time [sec], power [W], and energy [J] )

end\_z\_axis = 20.0

...

out\_silent = off

\*\*\*\*end of information input file\*\*\*\*

...[SCREEN OUTPUT]

...[SCREEN OUTPUT]

\*\*\*\*\* Stokes beam \*\*\*\*\*

out\_stokes : intensity and phase are on optical axis

Note that Stokes power is reset after each step

z	power	intens	phase	widthX	widthY	Icorner	Ndx/wX	Ndy/wY
0.000	1.53e-4	0.03907	0.000	0.05000	0.05000	1.9e-12	2.50	2.50
2.000	1.58e-4	0.07780	-0.0480	0.03791	0.03791	1.5e-13	2.66	2.66

...

20.00	1.57e-4	0.07338	-5.999	0.03981	0.03981	7.5e-14	3.14	3.14
-------	---------	---------	--------	---------	---------	---------	------	------

end Stokes beam

\*\*\*\*\* pump beam \*\*\*\*\*

out\_pump : intensity and phase are on optical axis

z	power	intens	phase	widthX	widthY	Icorner	Ndx/wX	Ndy/wY
0.000	1.534e6	3.907e8	0.000	0.05000	0.05000	0.01864	2.50	2.50
2.000	1.534e6	6.015e8	-0.0396	0.04030	0.04030	1.85e-3	2.50	2.50

...

20.00	1.534e6	3.923e8	-2.815	0.04992	0.04992	8.92e-4	2.50	2.50
-------	---------	---------	--------	---------	---------	---------	------	------

end pump beam

\*\*\*\* Time Profile and Plane Wave Approximation \*\*\*\*

time profile: pump and Stokes (F and B)

number of iterations per time display: 449.1

time	P_in	P_out	F_out	B_out	E_in	E_out
0.000	6.950	0.000	0.000	0.000	0.000	0.000
1.501e-9	4.437e5	1.497e5	7.51e-7	6.09e-7	2.33e-4	4.26e-5
2.999e-9	1.238e6	9.060e5	0.04132	0.05463	1.51e-3	7.95e-4
4.496e-9	1.530e6	1.492e6	177.3	183.6	3.68e-3	2.67e-3
5.994e-9	1.176e6	1.389e6	40.34	32.60	5.76e-3	4.91e-3
7.492e-9	6.256e5	8.628e5	0.02231	0.01793	7.10e-3	6.61e-3
8.990e-9	2.414e5	3.823e5	2.34e-5	2.09e-5	7.72e-3	7.52e-3
1.049e-8	6.931e4	1.248e5	4.97e-7	4.73e-7	7.93e-3	7.87e-3
1.199e-8	1.503e4	3.061e4	5.52e-8	5.33e-8	7.99e-3	7.97e-3
1.349e-8	2475	5681	8.51e-9	8.25e-9	8.00e-3	8.00e-3
1.498e-8	157.5	810.1	1.17e-9	1.14e-9	8.00e-3	8.00e-3

Total energies pump and Stokes.

Energy transmitted pump : 7.999e-3

Energy forward Stokes : 3.784e-7

Energy backward Stokes : 3.550e-7

$E_P + kP/kS \cdot (E_B + E_F) : 8.000e-3$

\*\*\*\*\*

Used DEFAULT values:

out\_debug = off

out\_data\_files = off

...  
...

reflection\_entrance\_stokes = 0.0

reflection\_exit\_stokes = 0.0

\*\*\*\*\*

Value of AUTOMATIC variables:

display\_step\_size\_z\_axis = 2

x\_spacing\_grid\_points = 0.003125

y\_spacing\_grid\_points = 0.003125

pump\_profile\_file = no file; profile is:  $\text{time}^2 \cdot \exp[-(1.15 \cdot \text{time} / \text{pulsewidth})^2]$

display\_time\_step = 1.49813e-09

spontaneous\_scattering = 0

\*\*\*\*\*

Information from the input file that was NOT used:

pump\_power = 2.50e6  
stokes\_power = 1.00e-19

The output file shown above is the shortest possible, since all output parameters are off by default. Since the screen output is repeated in the output file, no information is lost by setting out\_silent=on. For this setting, screen output is suppressed and the program can run in the background or in a batch job. Parallel processing is possible by running the program for different input files in the background.

Graphical output is not provided by the program, but setting out\_data\_files=on gives data files with extension dto, which can be easily read by various graphical software packages (e.g. UNIGRAPH).

## LIST OF INPUT PARAMETERS

All parameters are listed in the file full.inp. If the program is modified, full.inp should also be modified to provide an up-to-date list of parameters. Here follows the contents of full.inp:

Input file for the Stimulated Raman Scattering program: rambo.

This is an example input file showing all the possible entries.  
The values are only listed as an example and do not reflect a realistic experiment.  
The default values, if available, are listed in the comments.

## GENERAL INPUT PARAMETERS

```
end_z_axis = 20.0 [cm] /* length Raman cell */

pump_place_x_focus = 10.0 [cm] /* position of focus (in x-z plane) */
pump_x_width/2 = 0.0572 [cm] /* beam width (half diameter at 1/e2 points) */
width_at_focus = off /* on or off; width is specified at focus or entrance;
                        default: off */
pump_place_y_focus = 10.0 [cm] /* default: pump_place_x_focus */
pump_y_width/2 = 0.0572 [cm] /* default: pump_x_width/2 */
pump_beam_quality = 1.0 /* factor = 1/M2 <= 1 ; contains ratio focus-width or
                        divergence compared to a diffraction limited beam; default: 1.0 */
pump_hermite_x = 1 /* order Hermite polynomial; default: 0 */
pump_hermite_y = 0 /* default: 0 */
/* these two entries are used if the hermite orders are 0 and 0 */
pump_laguerre_angular = 0 /* angular order Laguerre mode; default: 0 */
pump_laguerre_radial = 0 /* radial order Laguerre mode; default: 0 */

pump_wavenumber = 6.165e4 [1/cm] /* wavenumber in medium (not free space) */
stokes_wavenumber = 6.165e4 [1/cm] /* wavenumber in medium (not free space);
                                     default: pump_wavenumber */

raman_gain_stokes = 4.91e-10 [cm/W]

random_seed = 0.1 /* seed for random generator: >0 and <1; default: 0.1234 */

#average = 1 /* number of runs to average; default: 1 */
```

BEAM PROPAGATION METHOD : uses 2-dim grid for beam profile

beam\_propagation = on /\* on or off; skip this method when off \*/  
use\_symmetry = on /\* on or off; on increases speed; default: on \*/

step\_size\_z\_axis = 0.2 [cm] /\* step size of FD-method; default: auto \*/  
display\_step\_size\_z\_axis = 2.0 [cm] /\* value or auto; default: auto \*/  
variable\_step = off /\* on, off, or auto; default: auto \*/  
var\_step\_criterium = 1.0 /\* used if variable\_step is auto; limits step size;  
default: 1.0 \*/

/\* these two entries are used if variable\_step is on \*/  
var\_step\_size = 0.1 0.05 0.02 0.02 0.02 0.05 0.1 [cm]  
var\_step\_start\_z = 0.0 5.0 7.0 8.0 12.0 13.0 15.0 [cm]

#grid\_points\_on\_axis = 30 /\* the same for the x- and y-axis; default: 40 \*/  
/\* grid spacing can be obtained automatically if grid\_adjustment is pump \*/  
x\_spacing\_grid\_points = 0.0055 [cm] /\* size delta x or auto; default: auto \*/  
y\_spacing\_grid\_points = 0.005 [cm] /\* size delta y or auto; default: auto \*/  
grid\_adjustment = pump /\* none, pump, stokes, or focus; default: pump \*/  
stokes\_grid = off /\* on or off; separate curvature for stokes; default: off \*/  
/\* these four entries are used if grid\_adjustment is 'focus' \*/  
grid\_place\_x\_focus = 10.0 [cm]  
grid\_reduction\_x\_focus = 0.02 /\* smaller than one \*/  
grid\_place\_y\_focus = 10.0 [cm]  
grid\_reduction\_y\_focus = 0.02 /\* smaller than one \*/

pump\_power = 2.50e6 [W] /\* more than one value is allowed \*/  
stokes\_power = 1.00e-19 [W] /\* more than one value is allowed, but use the  
same number as with pump\_power \*/  
stokes\_noise = off /\* on or off; spontaneous Stokes power; default: off \*/

stokes\_place\_x\_focus = 10.0 [cm] /\* default: pump\_place\_x\_focus \*/  
stokes\_x\_width/2 = 0.0572 [cm] /\* default: pump\_x\_width/2 \*/  
stokes\_place\_y\_focus = 10.0 [cm] /\* default: pump\_place\_x\_focus \*/  
stokes\_y\_width/2 = 0.0572 [cm] /\* default: pump\_x\_width/2 \*/  
stokes\_hermite\_x = 0 /\* order Hermite polynomial; default: 0 \*/  
stokes\_hermite\_y = 0 /\* default: 0 \*/

/\* these two entries are used if the hermite orders are 0 and 0 \*/  
stokes\_laguerre\_angular = 0 /\* angular order Laquerre mode; default: 0 \*/  
stokes\_laguerre\_radial = 1 /\* radial order Laquerre mode; default: 0 \*/

pump\_shape = normal /\* normal, donut, tophat, smooth\_tophat, GSM;  
default: normal \*/  
stokes\_shape = normal /\* normal, donut, tophat, smooth\_tophat, GSM;

```
default: normal */
fixed_power_GSM = on /* used if beam_shape is GSM; default: on */

edge_transparency = off /* on or off; default: off */
edge_absorption = 0.1 [1/cm] /* absorption coefficient; default: 0.0 */
/* #edge_points is used when edge_absorption is greater than 0.0 */
#edge_points = 1 /* normally one, greater or equal to one; default: 1 */
low_pass_filter = off /* on or off; default: off */

fully_explicit = 0.2 /* if dz/kdx^2 < fully_expl, the f.e. method is used;
default: 0.0 */

TIME-PROFILE AND PLANE-WAVE APPROXIMATION

time_plane_wave = on /* on or off; time profile and plane wave approx. */

pump_profile_file = auto /* name data file; default: auto */
pulse_width = 5e-9 [s] /* Used when pump_profile_file is auto; FWHM */
pump_energy = 8.0e-3 [J] /* scales the pump power to this energy;
more than one value is allowed */

#intervals_z_axis = 200 /* z-axis is divided in parts of equal lengths;
default: 200 */
gain_window = 0.1 /* 0<=factor<1; amplification only for
gain > gain_window*gain_max; default: 0.0 */
gain_focusing = 1.674 /* factor for describing gain_foc; default: 1.3 */

display_time_step = 0.25e-9 [sec] /* value or auto; default: auto */

spontaneous_scattering = 1e-13 /* factor, works only at entrance;
Stokes_power is factor * pump_power; default: auto */
spontaneous_power = 1e-7 [W] /* used when transient_gain is off;
default: 1e-7 [W] */

refractive_index = 1.0 /* for speed of light in Raman cell; default: 1.0 */

reflection_entrance_stokes = 0.0 /* fraction backward to forward Stokes;
default: 0.0 */
reflection_exit_stokes = 1.0 /* fraction forward to backward Stokes;
default: 0.0 */

transient_gain = on /* on or off, with off the steady-state gain is used;
default: off */
raman_linewidth = 0.2 [1/cm] /* linewidth: Full Width Half Maximum */
```

```
pump_linewidth = 0.0 [1/cm] /* linewidth: Full Width Half Maximum */
mode_spacing = 0.05 [1/cm] /* spacing of longitudinal modes pump */
langevin_noise = on /* on or off; noise in the Raman polarization */
correct_fresnel# = off /* on or off; correction in noise for Fresnel number */

ground_state_depletion = on /* on or off, with on gaingrid is used;
                             default: off */
degeneracy_ratio = 0.0 /* ratio, degeneracy ground state divided by
                         degeneracy excited state */
atom_density = 2.53e19 [1/cm^3] /* number density of atoms or molecules */

brillouin_scattering = off /* on or off, with on SBS is included */
brillouin_gain_stokes = 23.8e-9 [cm/W] /* gain Stimulated Brillouin Scat. */
brillouin_linewidth = 0.0014 [1/cm] /* linewidth: Full Width Half Maximum */

second_order_raman = off /* on or off; on for cascade second order Raman */
raman_gain_stokes2 = 4.8e-10 [cm/W] /* gain second order SRS */
stokes2_wavenumber = 2.33e4 [1/cm] /* wavenumber in medium (not free space) */
reflection_entrance_stokes2 = 1e-4 /* fraction backward to forward Stokes */
reflection_exit_stokes2 = 5e-4 /* fraction forward to backward Stokes */
```

#### OUTPUT SPECIFICATIONS

```
out_silent = on /* off means output to stdout, on means silent;
                 default: off */

out_intensity = x /* off or direction: x, y, or xy;
                  the intensity along direction is shown; default: off */
out_phase = off /* off or direction: x, y, or xy;
                 the phase along direction is shown; default: off */
out_2D_intensity = 10.0 /* off or position(s) on z-axis; default: off */
out_wavefront = on /* on or off; M^2, curvature, etc; default: off */

out_amp_grid = on /* on or off; shows amplification grid; default: off */
out_vol_grid = on /* on or off; shows volume of z-grid; default: off */
out_power_time = off /* off or time point(s) to display powers in cell;
                     default: off */
out_polar_time = 1e-9 /* off or time point(s) to display polarization;
                      default: off */
out_polar_index = 100 /* off or index of z-position(s) to display
                      polarization[z_index] versus time; default: off */

out_data_files = off /* on or off; writes information to data files with
                      extension .dto; default: off */
```

out\_reduce\_data = auto /\* off, auto, or reduction factor (integer);  
reduces data in data files; default: auto \*/

out\_debug = off /\* on or off; shows debugging information; default: off \*/

## DETAILS OF THE PROGRAM

The program is written in the language C using the version of Kernighan and Ritchie and not the new ANSI-C version. Using K&R-C means that the program should be portable to all computer systems with a C-compiler. For instance, we have ported the program to an MS-DOS PC, where the program ran (although not so fast) with only a few modifications, which were mostly caused by the crippled memory management of the PC.

The source code of almost 10.000 lines is divided among 14 files not counting the header files. A special header file is `ramandef.h` that contains the constant definitions:

```
/* Header file that contains the definitions of the raman program. */

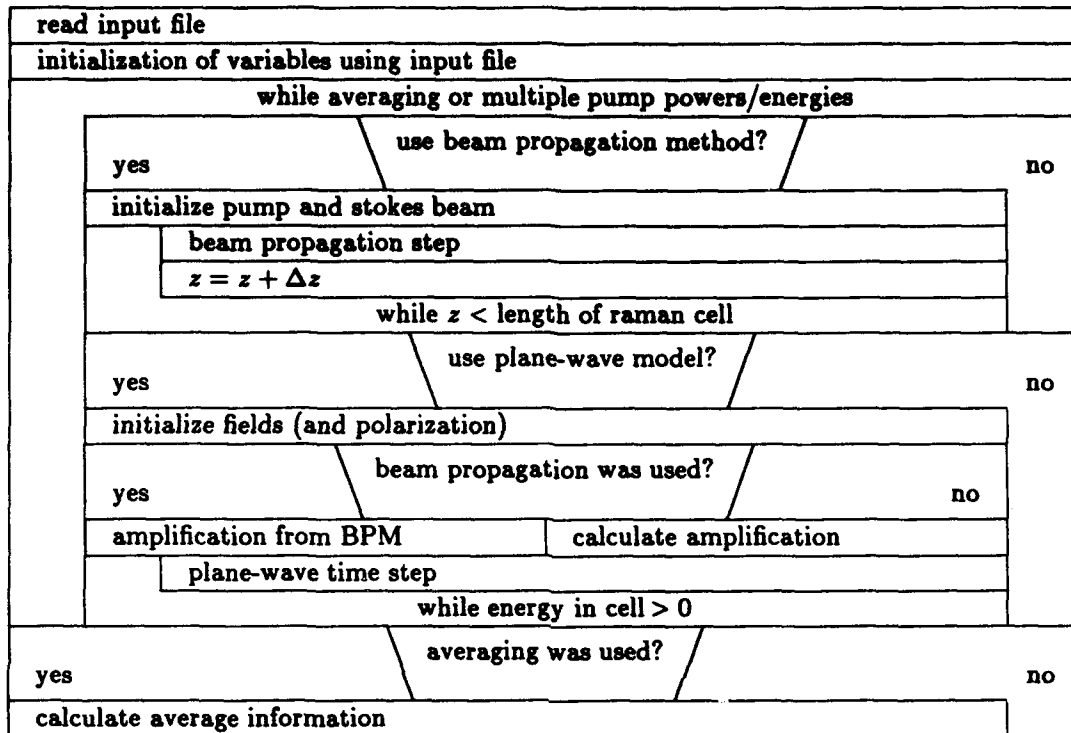
#define LOCAL_VAR 0 /* 0 for maximum use of global memory (saves memory),
    1 for maximum use of local memory (increases speed) */
#define NTRD 121 /* the maximum size of the beam array */
#define NZ 801 /* the max. number z-intervals in the plane wave approx. */
#define PI 3.141592654
#define h_Planck 6.6262e-34 /* J.s */
#define c_light 2.9979e10 /* cm/s */
#define ONE 1.00001 /* compensates round-off in comparisons */
#define SIGNAL -1.234567 /* signal value */
#define NLOWPASS 2 /* low_pass_filter after 2 steps */

#define equal(z1, z2) (ONE*(z1)>=(z2) && ONE*(z2)>=(z1)) /* equal */
```

The 14 source files are in alphabetic order

<code>average.c</code>	contains functions for averaging
<code>inputfil.c</code>	functions for reading the input file
<code>memman.c</code>	for memory management
<code>outfil.c</code>	basic functions for writing to the output file
<code>ramidim.c</code>	plane-wave model, core functions
<code>ramidout.c</code>	plane-wave model, output functions
<code>ramanout.c</code>	output functions for beam propagation method
<code>ramcontr.c</code>	contains upper level functions
<code>ramfunc.c</code>	beam propagation method, core functions
<code>ramfunc2.c</code>	beam propagation method, core functions
<code>ramp.c</code>	highest level, contains <code>main()</code>
<code>randomf.c</code>	random generators
<code>rcomplex.c</code>	functions for complex numbers
<code>wavefron.c</code>	beam wavefront analysis

At the outermost level, the program works according to the following flow-diagram:



## REPORT DOCUMENTATION PAGE

(MOD-NL)

1. DEFENSE REPORT NUMBER (MOD-NL) TD93-1737	2. RECIPIENT'S ACCESSION NUMBER	3. PERFORMING ORGANIZATION REPORT NUMBER FEL-93-A135
4. PROJECT/TASK/WORK UNIT NO. 22459	5. CONTRACT NUMBER A90KL674	6. REPORT DATE JUNE 1993
7. NUMBER OF PAGES 85 ( INCL. 3 APPENDICES, EXCL. RDP & DISTRIBUTION LIST)	8. NUMBER OF REFERENCES 39	9. TYPE OF REPORT AND DATES COVERED
10. TITLE AND SUBTITLE THEORY AND MODELING OF STIMULATED RAMAN SCATTERING		
11. AUTHOR(S) J.C. VAN DEN HEUVEL		
12. PERFORMING ORGANIZATION NAME(S) AND ADDRESS(ES) TNO PHYSICS AND ELECTRONICS LABORATORY, P.O. BOX 96864, 2509 JG THE HAGUE OUDE WAALSDORPERWEG 63, THE HAGUE, THE NETHERLANDS		
13. SPONSORING/MONITORING AGENCY NAME(S) ROYAL NETHERLANDS ARMY, DMKL/OMAT/KIO		
14. SUPPLEMENTARY NOTES THE CLASSIFICATION DESIGNATION ONGERUBRICEERD IS EQUIVALENT TO UNCLASSIFIED.		
15. ABSTRACT (MAXIMUM 200 WORDS, 1044 POSITIONS) A THREE-DIMENSIONAL FINITE DIFFERENCE METHOD IS PRESENTED FOR THE PROPAGATION OF BEAMS FOCUSED BY AN ASTIGMATIC LENS. THE METHOD IS USED FOR THE MODELING OF A RAMAN AMPLIFIER THAT USES ASTIGMATIC LENSES. WITH THIS METHOD, THE EFFECT OF GAIN FOCUSING ON THE AMPLIFICATION IS STUDIED. THE NUMERICAL RESULTS SHOW A GOOD CORRESPONDENCE WITH ANALYTICAL MODELS IN THE RANGE WHERE THESE MODELS ARE APPLICABLE. THE TRESHOLD POWER OF STIMULATED RAMAN SCATTERING (SRS) HAS BEEN CALCULATED FOR VARIOUS NONDIFFRACTION-LIMITED PUMP BEAMS USING THE NUMERICAL MODEL. IT IS SHOWN THAT THE THRESHOLD POWER, FOR A TIGHTLY FOCUSED BEAM, DEPENDS ON THE $M^2$ FACTOR THAT IS RELATED TO THE PUMP BEAM QUALITY. ADDITIONALLY, THE INFLUENCE OF THE EXACT PUMP BEAM PROFILE ON THE THRESHOLD IS SMALL. THEREFORE, THE $M^2$ FACTOR IS A USEFUL PARAMETER FOR ANALYZING THE EXPERIMENTAL THRESHOLD. WE SHOW THAT THE MEASURED SRS THRESHOLDS IN METHANE CORRESPOND WITH THE CALCULATED THRESHOLDS. AN ASTIGMATIC FOCUS HAS BEEN USED TO INCREASE THE CONVERSION EFFICIENCY OF A RAMAN CELL AT HIGH PUMP ENERGY. EXPERIMENTAL AND NUMERICAL RESULTS SHOW THAT THE INCREASED CONVERSION IS DUE TO THE REDUCTION OF CASCADE SECOND ORDER STOKES. IT IS SHOWN THAT OTHER EFFECTS, NAMELY BRILLOUIN SCATTERING, ANTI-STOKES GENERATION, AND GROUND-STATE DEPLETION ARE NEGLIGIBLE FO OUR EXPERIMENTAL SETUP.		
16. DESCRIPTORS METHANE LASERS COMPUTERIZED SIMULATION		IDENTIFIERS ND:YAG WAVELENGTH CONVERSION STIMULATED RAMAN SCATTERING EYE-SAFE LASERS
17a. SECURITY CLASSIFICATION (OF REPORT) ONGERUBRICEERD	17b. SECURITY CLASSIFICATION (OF PAGE) ONGERUBRICEERD	17c. SECURITY CLASSIFICATION (OF ABSTRACT) ONGERUBRICEERD
18. DISTRIBUTION/AVAILABILITY STATEMENT  NO RESTRICTIONS		17d. SECURITY CLASSIFICATION (OF TITLES) ONGERUBRICEERD